

## Anion-hosting cathodes for current and late-stage dual-ion batteries

Miao Zhang<sup>1,2†</sup>, Wenyong Zhang<sup>2‡</sup>, Fan Zhang<sup>2\*</sup>, Chun-Sing Lee<sup>3</sup> & Yongbing Tang<sup>2\*</sup>

<sup>1</sup>School of Chemistry and Materials Science, Guangdong University of Education, Guangzhou 510303, China;

<sup>2</sup>Advanced Energy Storage Technology Research Center, Shenzhen Institute of Advanced Technology, Chinese Academy of Sciences, Shenzhen 518055, China;

<sup>3</sup>Center of Super-Diamond and Advanced Film (COSDAF), City University of Hong Kong, Kowloon 999077, China

Received November 30, 2023; accepted February 6, 2024; published online March 6, 2024

Anion-hosting cathodes capable of reversibly storing large-size anions play a leading role in dual-ion batteries (DIBs). The purpose of the present review is to summarize the most promising anion-hosting cathodes for current and late-stage DIBs. This review first summarizes the developments in conventional graphite cathodes, especially the latest advances in the graphite-related research. Next, organic cathodes for the anion storage are discussed, including aromatic amine polymers, heterocyclic polymers, bipolar compounds, and all-carbon-unsaturated compounds. Then, the review focuses on the conversion-type cathodes with high theoretical specific capacities. Finally, the future research directions of the cathodes of DIBs are proposed.

**dual-ion batteries, organic cathodes, graphite cathodes, conversion-type cathodes**

**Citation:** Zhang M, Zhang W, Zhang F, Lee CS, Tang Y. Anion-hosting cathodes for current and late-stage dual-ion batteries. *Sci China Chem*, 2024, 67: 1485–1509, <https://doi.org/10.1007/s11426-023-1957-3>

### 1 Introduction

Green energy sources such as wind, solar, and tidal energy are environmentally-friendly and have the potential to mitigate several problems associated with fossil fuels [1]. However, because renewable energy is dependent on the natural environment, the power supply is unpredictable and unstable [2,3]. Therefore, ensuring a reliable supply of electricity to a microgrid by using green energy sources is difficult [4]. To address the aforementioned problems, renewable energy power plants have been outfitted with energy storage technologies [5,6]. Current researches are focusing on exploring novel and low-cost cathode/anode materials based on lithium-ion batteries (LIBs) [7,8] and post-LIBs (sodium-, potassium-, calcium-, magnesium-, and alumini-

num-ion batteries) [9,10]. Furthermore, novel energy storage concepts have also been studied to develop energy storage devices (ESDs) that have low-carbon, environmental-friendliness, and exceptional performance [11–14].

Dual-ion batteries (DIBs), in which anions and cations from the electrolyte react with the cathodes and anodes simultaneously, have received considerable research attention in recent years [6,15–17]. Anionic reactive electrodes on the cathode and cationic reactive electrodes on the anode make up DIBs, which differs from LIBs in that the electrolyte's anions and cations react concurrently during the battery reaction. The cathode and anode of a DIB, which uses graphite as the cathode, aluminum (Al) as the anode, and LiPF<sub>6</sub> in carbonate as the electrolyte, are utilized as an example [18]. The charging process involves the interlayering of the PF<sub>6</sub><sup>-</sup> into the graphite layer and the alloying of Li<sup>+</sup> with the Al anode. Anions and lithium ions are removed from the electrode and returned to the electrolyte during the discharge

<sup>†</sup>These authors contributed equally to this work.

\*Corresponding authors (email: [fan.zhang1@siat.ac.cn](mailto:fan.zhang1@siat.ac.cn); [tangyb@siat.ac.cn](mailto:tangyb@siat.ac.cn))

process, which is the inverse of the charging process. Compared with conventional LIBs, DIBs provide the following benefits.

**Lower cost of cathodes.** Cathode materials for LIBs typically include Co and Ni, which have disadvantages such as unequal resource allocation, high price, and environmental pollution during the manufacturing process [19]. The cost of these cathode materials is between 40% and 50% of the total cost of a LIB [20]. However, the typically graphite as the cathode material of DIBs costs considerably lower than that of LIBs [21].

**Improved low-temperature performance.** The specific capacity, energy density (ED), and power density (PD) of LIBs at low temperature (below  $-40^{\circ}\text{C}$ ) are only 1%–12% of those at room temperature, which is insufficient for applications [22]. This phenomenon could be attributed to the decrease of ion conductivity of the electrolyte and the increase of interface charge transfer resistance [23,24]. However, DIBs, unlike LIBs, are anion and cation systems that act simultaneously during charging and discharging. The weak anion–solvent interaction in DIBs minimizes the anion de-solvation barrier, allowing the weak anion solvation effect to avoid kinetic barriers during low-temperature operations [22].

**Battery system universality.** The battery system based on the dual-ion reaction is not confined to lithium-ion DIBs (Li-DIBs). Novel battery systems such as sodium, potassium, magnesium, zinc, aluminum, and calcium DIBs (Na-DIBs [25], K-DIBs [26–30], Mg-DIBs [31,32], Zn-DIBs [33], Al-DIBs [34–37], and Ca-DIBs) [38–40] with the excellent cycle stability and high-rate performance can be realized. The dual-ion working mechanism can be used for the development of novel battery systems [41].

In DIBs, the only source of cations and anions is the electrolyte [42,43]. Therefore, the performance of DIBs is partially governed by the electrolyte, which a crucial component of the active mass [44,45]. Numerous charge carriers, including  $\text{Li}^+$ ,  $\text{Na}^+$ , and  $\text{K}^+$  [46], are available for the anode side of DIBs [47]. Anode materials, which store charge carriers, contain three reaction mechanisms (insertion, alloying, and conversion) for the storage of cations [48]. Numerous anode materials have been extensively developed based on these three mechanisms to store  $\text{Li}^+$ ,  $\text{Na}^+$ ,  $\text{K}^+$ , etc. [49–51]. Theoretically, the anode materials that are used in most non-aqueous metal-ion batteries, such as LIBs, may also be used in DIBs [52–56]. However, unlike anode materials, the cathode materials of DIBs need to store large-size anions (such as  $\text{PF}_6^-$ ,  $\text{BF}_4^-$ ,  $\text{FSI}^-$ ,  $\text{FTFS}^-$ ,  $\text{TFSI}^-$ , and  $\text{ClO}_4^-$ ) [57–59], which show slower ion-diffusion rates than those of alkali metal ions, resulting in inferior electrochemical properties [3,60].

Currently, graphite is the most commonly used cathode material because of its ability to form graphite intercalation

compounds (GICs) [61,62]. Graphite cathodes have several benefits, such as being inexpensive, safe, and eco-friendly [59,63]. High anion intercalation potential also contributes to the high operating voltage of graphite-based DIBs, which is typically above 4.5 V, which is advantageous for high energy density [64]. However, the high working voltage results in continuous electrolyte decomposition and low Coulombic efficiency (CE) [65]. Furthermore, the lack of active sites of graphite for anions causes insufficient capacity ( $\sim 100 \text{ mAh g}^{-1}$ ), and the repeated de/intercalation of bulky anions and solvents results in severe graphite exfoliation in the cathode and poor cycle stability [16,66].

Therefore, enhancing the properties of graphite and exploring superior alternatives, which reversibly store anions, for DIBs are critical [75]. This review summarizes the current progress in improving the capacity and CE of DIBs from the perspective of the development of cathode materials, which can reversibly store anions (Figure 1). First, we cover the DIB system developed with graphite as the cathode and detail strategies used to improve the electrochemical performance of graphite-cathode-based DIBs (G-DIBs). Next, the compounds represented by organic cathodes are introduced. We then elaborate on the development of organic cathode materials in DIBs. Subsequently, we present conversion-type cathode materials with higher specific capacities that can accommodate anions. Finally, future trends based on our understanding of cathodes of DIBs are presented.

## 2 Graphite-based cathodes

### 2.1 Discovery and characterization of graphite intercalation compounds (GICs)

Researchers have developed acceptor-type, graphite-based batteries that can be applied in gas adsorption, desalination, and electrochemical energy storage [20]. The first GIC,  $\text{H}_2\text{SO}_4$ -GIC, was discovered in 1840, followed by  $\text{HClO}_4$ -GICs and  $\text{HNO}_3$ -GICs in 1925 [20]. In 1938, Rüdorff and Hofmann [76], for the first time, applied the reversible intercalation of  $\text{HSO}_4^-$  anions in graphite in batteries. McCullough *et al.* [77] introduced a rechargeable battery using two graphite electrodes and a non-aqueous electrolyte in 1989. Subsequently, the ionic liquid was used as an electrolyte for reversible oxidation and reduction intercalation of various anions and cations in graphite electrodes [78]. Current research is focusing on understanding the intercalation mechanism of anions between graphite layers for practical applications in high ED batteries [79].

Earlier studies on the anion intercalation phenomena in graphite mainly used X-ray diffraction (XRD) to indirectly observe the structural modifications of graphite induced by the intercalating species following a staging mechanism [80].

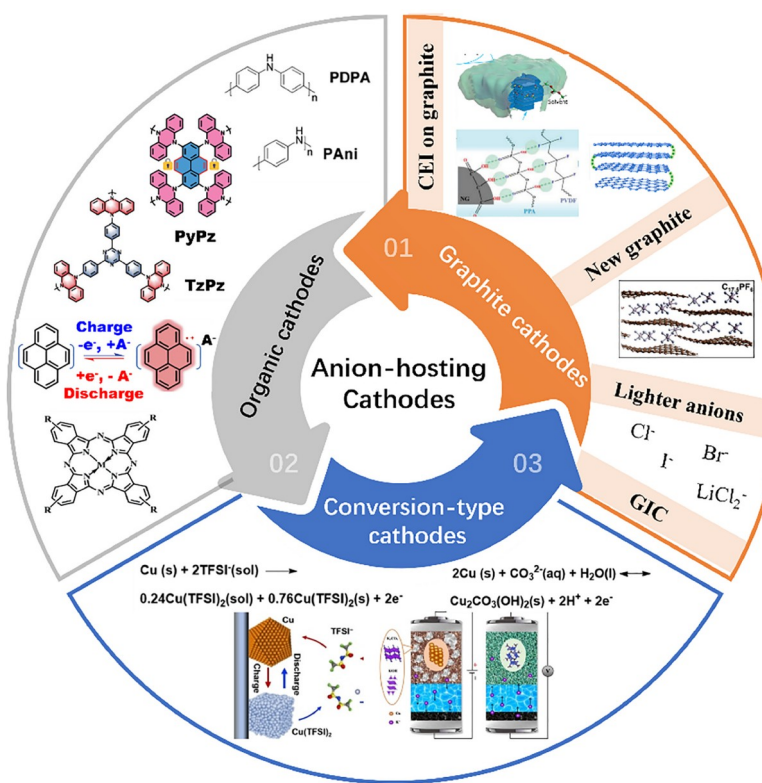


**Figure 1** Schematics of anion-hosting cathodes of DIBs. Graphs for graphite cathodes. Reproduced with permission [67]. Copyright 2023, Wiley-VCH. Reproduced with permission [68]. Copyright 2021, Elsevier. Reproduced with permission [69]. Copyright 2020, Wiley-VCH. Graphs for organic cathodes. Reproduced with permission [70]. Copyright 2022, Wiley-VCH. Reproduced with permission [71]. Copyright 2021, Wiley-VCH. Reproduced with permission [72]. Copyright 2021, the Royal Society of Chemistry. Graphs for conversion-type cathodes. Reproduced with permission [73]. Copyright 2022, Wiley-VCH. Reproduced with permission [74]. Copyright 2022, Wiley-VCH (color online).

To figure out the current intercalation stage of GICs from this indirect measurement, models and theoretical calculations are needed [81]. A straight technique, on the other hand, shows the formation process of GICs without using simulations or mathematical calculations. For example, small angle X-ray scattering (SAXS) is a good way to study the GIC formation because it can directly find the periodic repeat distance ( $I_c$ ). This helps us to study the staging and its intermediate phase changes very accurately [82].

Subsequent studies used Raman and optical microscopy to observe the GIC formation [83]. However, these techniques are limited to the test of the surface of the material, and can only provide part of the information of the intercalation of anions between bulk graphite [84]. *Operando* X-ray scattering from SAXS to wide angles (WAXS) [85] can provide a comprehensive understanding of intermediate phase transitions during the formation of GICs by facilitating the determination of the relationship between structural modification and electrochemical behavior of the graphite cathode.

Further development of G-DIBs will depend on the development of *in-situ* testing technology. Advanced *in-situ* characterization technologies not only help to understand the relevant mechanism of anions in the graphite layer but also

help to design and develop better graphite cathode materials for high-performance G-DIBs.

## 2.2 Smaller anions for graphite cathodes

$\text{PF}_6^-$ ,  $\text{BF}_4^-$ ,  $\text{FSI}^-$ ,  $\text{FTFS}^-$ ,  $\text{TFSI}^-$ , and  $\text{ClO}_4^-$  are commonly used anions to react with graphite cathodes in DIBs [7]. New acceptor-type GICs can be used as cathode materials for DIBs [86,87,88], whereas halogens ( $\text{Cl}^-$ ,  $\text{Br}^-$ ,  $\text{I}^-$ ) with smaller size are being developed as anion charge carriers. For example, Wang *et al.* [89] reported the co-intercalation of  $\text{Cl}^-$  and  $\text{Br}^-$  into the graphite cathode forming a compound of  $\text{C}_{3.5}[\text{Br}_{0.5}\text{Cl}_{0.5}]$ , giving a high discharge capacity of 243  $\text{mAh g}^{-1}$  in an aqueous Li-based full battery. Similarly,  $\text{Cl}^-$  and  $\text{I}^-$  can be also intercalated into the graphite cathode and the specific capacity can reach 291  $\text{mAh g}^{-1}$  in a Zn metal battery [90]. The specific capacity of halogens intercalated into graphite can even reach 605.7  $\text{mAh g}^{-1}$  in a concentrated  $\text{ZnCl}_2/\text{ZnBr}_2/\text{Zn(OAc)}_2$  aqueous electrolyte [91].

A smaller mass of anions intercalated into graphite, on the one hand, helps to reduce the quality of the electrolyte and the quality of the active material; on the other hand, a smaller volume of anions is intercalated into the graphite cathode or will obtain a higher theoretical capacity based on the graphite

cathode, thereby significantly improving the ED of G-DIBs.

### 2.3 New graphitic carbon materials

The intercalation behaviors of anions at the graphite cathode have been studied extensively [5,92]. Several features of graphite, including particle size, morphology, and crystallinity, have been shown to affect the anion intercalation performance [63,93–98]. The process of anion absorption is enhanced when the level of graphite crystallinity increases. Specifically, the specific capacity of the electrode is directly proportional to the degree of graphitization exhibited by the graphite material. In addition, the capacity of graphite is minimally affected by the height of crystal size. Furthermore, the utilization of graphite with reduced radius and increased specific surface area enables improved capacity and rate performance [20]. In the other hand, the physical or chemical treatment of graphite can also have an impact on the anion storage characteristics. For example, Tatsumi *et al.* [99] found that the introduction of nano-sized pores into graphene sheets could provide a large capacity of  $147 \text{ mAh g}^{-1}$  through the intercalation of  $\text{PF}_6^-$ . In another case, simple acidification treatment generates edge-rich flake-stacked graphite, allowing  $\text{AlCl}_4^-$  to diffuse into the interior flake-stacked layers, shortening the diffusion pathway, and improving intercalation behaviors in graphite electrodes for aluminum DIBs [100].

To increase capacity, Martha *et al.* [101] devised an ap-

proach that combines the graphitic intercalation (battery-type) with the surface storage from non-graphitic carbons (capacitor-type). An appropriate composite ratio of graphitic and non-graphitic carbon can greatly improve the specific capacity and cycle life. Modulating the degree of oxidation of graphite has an impact on the layer spacing and oxygen content, therefore influencing the intercalation point and specific capacity of the anions [102]. Electrode materials possessing greater interlayer spacing may offer a potential solution to address the issues of inadequate CE and cycle stability in DIBs, by enabling the reversible storage of bigger anions. For instance, mesocarbon microbeads with a wider interlayer spacing exhibited a higher specific capacity, higher CE, and longer cycle life than that with the smaller ones [103].

Graphitization degree is important for lowering the excessive voltage of anion storage in carbon materials, as revealed by DFT (density functional theory) calculations. Three common carbon structures were employed as proof-of-concept cathodes to test the viability of a locally ordered graphitized carbon (LOGC)-structured design technique for carbon-based cathodes in K-DIBs (Figure 2) [69]. Activated carbon (AC) is fully disordered (Figure 2a, 2b); graphite is nearly ordered (Figure 2d, 2e), and LOGC is a mixture of ordered graphite and disordered carbon (Figure 2g, 2h). DFT studies showed that the usual stage of AC (Figure 2a) for the anion storage at disordered carbon-based cathodes is near the margins of carbon nanosheets. Less than  $70 \text{ mAh g}^{-1}$  of

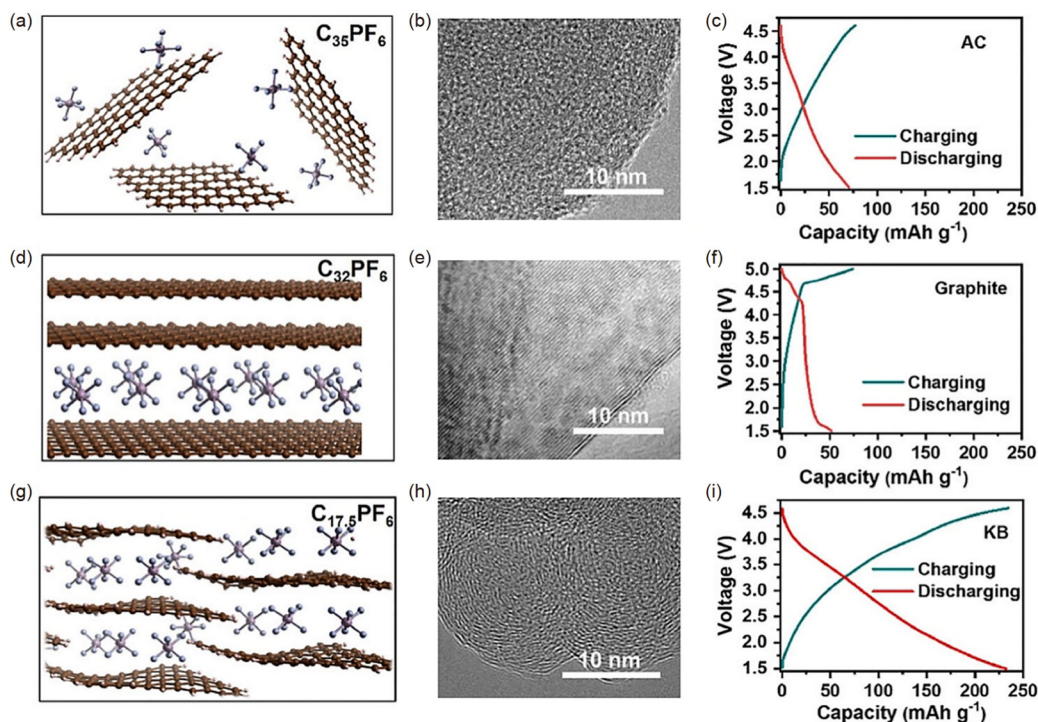


**Figure 2** Comparison between three typical carbon cathodes with different microstructures. Schematic anion storage mechanisms of disordered carbon (a), fully graphitized carbon (d), and LOGC (g), and HRTEM images of AC (b), graphite (e), and KB (h) and their individually typical galvanostatic charge-discharge curves (c, f, i). Reproduced with permission [69]. Copyright 2020, Wiley-VCH (color online).

discharge-specific capacity was achieved at the AC cathode. The specific capacity of anion intercalation in the graphite cathode, however, was  $127.6 \text{ mAh g}^{-1}$  due to the synergistic effect of intercalation and adsorption (Figure 2d). LOGC-structured Ketjen black (KB) cathodes increased the capacitive capacity of the carbon cathode due to their high specific surface area. Over  $232 \text{ mAh g}^{-1}$  of steady specific capacity was achieved in the K-DIB. It is possible that the LOGC and disordered carbon can lessen the strength of van der Waals interactions between graphene layers.

The design and characterization of graphite electrode materials, combined with theoretical calculation and simulation, will further promote the research and development of new and high-performance graphite cathodes. The design and regulation of graphite cathode structure is still an important component of the development of graphite materials.

#### 2.4 Cathode–electrolyte interface modification of graphite cathodes

Because reversible anion intercalation into graphite requires strong oxidative stability, highly concentrated electrolytes (HCEs) are commonly used in G-DIBs [104]. However, HCEs cannot create a stable cathode–electrolyte interface (CEI) layer, which is critical in the design of G-DIBs with high CE and long cycle life, necessitating electrolyte systems incorporated with salts and solvents that aid the formation of a stable CEI layer on graphite [105]. Various CEIs have been proposed to improve the CE and cycle life in G-DIBs (Table 1).

The most common and easiest method to obtain the CEI film is to generate it *in-situ* during the battery charging and

discharging. For instance, with the addition of the triallyl phosphate (TAP) monomer to electrolytes, Asfaw and Kotronia [106] reported the *in-situ* synthesis of a polymeric CEI layer. TAP improved the cycle life and CE of MoS<sub>2</sub>-graphite DIBs (Figure 3a). Yang *et al.* [107] used *tris(trimethyl-silyl)* phosphite (TMSP) as an electrolyte additive to enhance electrochemical performance (Figure 3b). Because TMSP may both scavenge hazardous species created by electrolytes and also provide a thin and uniform CEI layer on graphite. Moreover, various binders affect the CEI film formation and electrochemical performance. For example, Kotronia *et al.* [108] investigated the role of binders in the overall performance of a DIB. Compared with carboxymethyl cellulose (CMC), the poly(vinylidene fluoride-*co*-hexafluoropropylene) (PVdF-HFP) binder stabilizes the graphite cathode interface, decreases parasitic processes, reduces interfacial resistance and boosts the rate capability.

Compared with the CEIs formed *in-situ*, artificial CEI layers exhibit uniformity and controllable thickness; additionally, its electrochemical performance is better. Artificial CEI films may be inorganic, organic, or hybrids.

A robust CEI layer on the graphite surface with inorganic components has garnered increasing attention. For example, Li *et al.* [109] used an affordable and resource-rich clay montmorillonite (MMT) layer as the artificial CEI layer. Abundant Si–OH groups on the surface of MMT facilitated the dispersion of active materials during the application of slurry, and the high operating voltage of the DIBs caused the electrolyte breakdown; the resulting HF could react with SiO<sub>2</sub> in MMT, which prevented it from corroding battery components and improved the structural stability of the DIBs. The DIBs retained 100% capacity for 500 cycles at

**Table 1** Comparison of the electrochemical performance of graphite based on different CEIs

CEI composition on graphite cathode	Anode	CE/Type of DIB	Specific capacity@rate	Cycling capability
polymerized TAP [106]	MoS <sub>2</sub>	97%–99%  K-DIB	$\sim 70$ , $\sim 61$ , $\sim 58$ , $\sim 50$ , and $\sim 44 \text{ mAh g}^{-1}$ @25, 50, 100, 250, and 500 mA g <sup>-1</sup>	96% after 100 cycles@100 mA g <sup>-1</sup>
decomposed tris(trimethyl-silyl) phosphite (TMSP) [107]	graphite	99.5%  Li-DIB	101.3, 100.2, 100.1, 99.5, and 98.2 mAh g <sup>-1</sup> @1, 2, 5, 10, and 20 C	92.5% and 88.7%, after 3,000 cycles@10 and 20 C
MMT [109]		73% (1st)  Li-DIB	78.7, 76.9, and 71.6 mAh g <sup>-1</sup> @1, 2, and 4 C	100% after 500 cycles@2 C 99% after 1,000 cycles@5 C
Al <sub>2</sub> O <sub>3</sub> [110]	Protected Li metal	70%–99%  Li-DIB	$\sim 80 \text{ mAh g}^{-1}$ @0.1 A g <sup>-1</sup>	80% after 2,700 cycles@200 mA g <sup>-1</sup>
TiO <sub>2</sub> /Carbon Layer [111]		98%–99%  Li-DIB	69 mAh g <sup>-1</sup> @10 C 40 mAh g <sup>-1</sup> @20 C	78.9% for 10,000 cycles@5 C
g-C <sub>3</sub> N <sub>4</sub> /carbon [112]	Li metal	71% (1st), 95%  Li-DIB	$\sim 82 \text{ mAh g}^{-1}$ @1 C $\sim 71 \text{ mAh g}^{-1}$ @10 C	87% after 1,500 cycles@5 C
DTPMP layer [113]		97%  Li-DIB	50.1 mAh g <sup>-1</sup> @80 C 37.1 mAh g <sup>-1</sup> @100 C	80% after 3,000 cycles@1 C
polyphosphoric acid (PPA) nanofilms [67]	Li metal   Si	65.8% (1st)  Li-DIB	90 mAh g <sup>-1</sup> @10 C 50 mAh g <sup>-1</sup> @20 C 30 mAh g <sup>-1</sup> @100 C	80% after 2,000 cycles@1 C
Carboxylic anhydride functionality [68]	Li metal	64% (1st)  Li-DIB	103.8, 99.3, 92.7, and 88.8 mAh g <sup>-1</sup> @0.2 C, 0.5 C, 1 C and 2 C	80% after 1,000 cycles@2 C

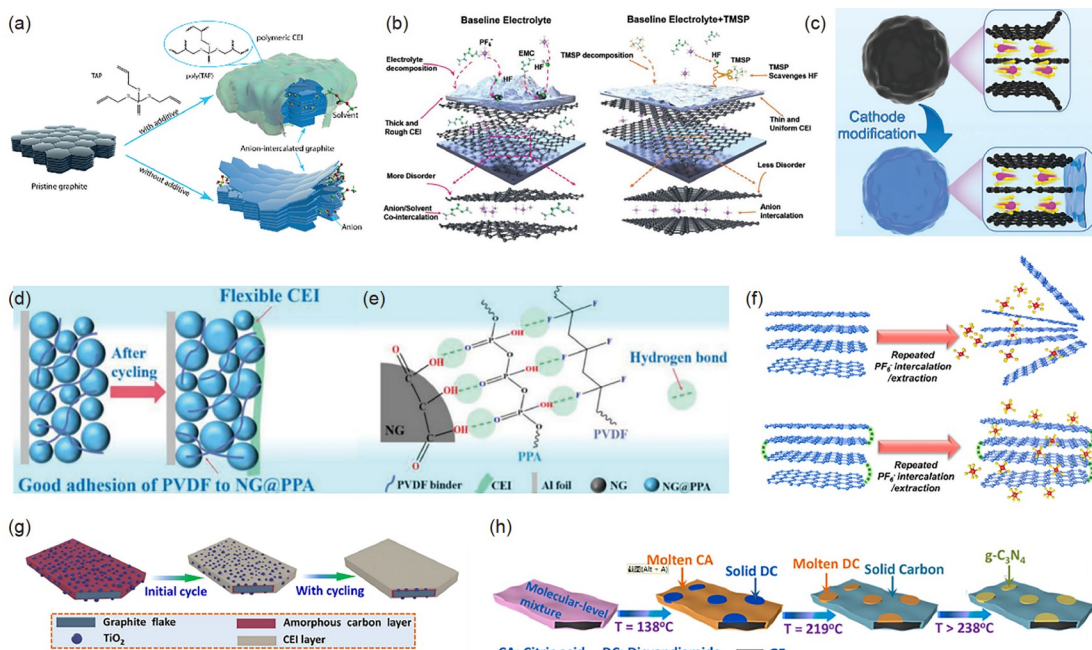


**Figure 3** (a) TAP [106] Open Access and (b) TMSP as the electrolyte additive for CEI. Reproduced with permission [107]. Copyright 2022, Wiley-VCH. (c) Al<sub>2</sub>O<sub>3</sub> modification strategy. Reproduced with permission [110]. Copyright 2022, Wiley-VCH. (d, e) PPA CEI. Reproduced with permission [67]. Copyright 2023, Wiley-VCH. (f) Interlink of graphite layers. Reproduced with permission [68]. Copyright 2021, Elsevier. (g) CEI layer of TO/GF and (h) g-C<sub>3</sub>N<sub>4</sub>/carbon. Reproduced with permission [111]. Copyright 2021, American Chemical Society. Reproduced with permission [112]. Copyright 2022, Elsevier (color online).

2 C, with the capacity retention being as high as 99% even after 1,000 cycles. In another case, a rigid interphase of Al<sub>2</sub>O<sub>3</sub> on graphite (Figure 3c) was reported to reduce structural deterioration. The low electrical conductivity of this protective Al<sub>2</sub>O<sub>3</sub> layer impeded the deposition of electrolyte-breakdown products [110]. In the all-climate temperature range of -25–40 °C, the resulting LG-DIBs were highly stable and exhibited a long cycle life, with capacity retention of 80% after 2,700 cycles at 200 mA g<sup>-1</sup>.

Organic molecules exhibit a high affinity toward graphite, and organic molecular membranes have a certain elasticity. Therefore, the artificial CEI obtained using organic molecules exhibits excellent performance. For instance, by implanting diethylenetriaminepenta(methylene-phosphonic acid) (DTPMP) on graphite, an *in-situ* electrochemistry-driven method for generating a bifunctional interphase was proposed [113]. The DTPMP-based interphase not only increased electrolyte-antioxidative stability but also aided the desolvation of PF<sub>6</sub><sup>-</sup> anions, which increased the ability to protect the graphitic structure twofold and contributed to the fast charging and ultralong cycling life. Zhang et al. [67] used an artificial CEI technique involving the incorporation of polyphosphoric acid (PPA) nanofilms on the graphite cathode through hydrogen bonding (Figure 3d and 3e). In addition, the problem of graphite layer peeling can also be solved by the chemical link of graphite surface groups. For example, selective incorporation of carboxylic anhydride functional groups between graphite layers can achieve a

stabilizing effect on the crystal structure (Figure 3f) [68].

An effective graphite cathode CEI film can also be developed by combining one or more substances. For instance, a highly efficient strategy for achieving stable CEI in secondary batteries involves the dissolution–precipitation and calcination. TiO<sub>2</sub> nanoparticles are distributed uniformly and bound tightly to the graphite flake surface, partitioning it into nanodomains (Figure 3g) [111]. This arrangement results in an ultralong-term cyclic ability resulting from the stable CEI layer and reduced electrolyte decomposition. Another strategy was the g-C<sub>3</sub>N<sub>4</sub>/carbon CEI layer with ultrafine g-C<sub>3</sub>N<sub>4</sub> imbed in carbon (Figure 3h), which allowed DIBs to maintain the graphite capacity with the increase in the interfacial binding strength [112].

In summary, the CEI modification of graphite is effective in optimizing the performance of G-DIBs. *In-situ* CEI has the advantage of a simple method, but uncontrolled *in-situ* polymerization will lead to uneven CEI films on the graphite surface, resulting in limited performance improvement. *Ex-situ* CEI includes electrodeless CEI, organic CEI and composite CEI, which have the characteristics of dense and strong, and graphite cathodes based on this type of CEI have good cycle stability. However, these CEI films generally require a certain preparation process. Subsequent methods for obtaining effective CEI membranes by simple preparation methods can be developed.

To summarize this section, graphite cathode materials are the most widely studied and applied materials in DIBs. In

recent years, the research interest of graphite cathodes has been gradually extended from the graphite structure modification to small anion electrolytes, new GIC characterization methods, graphite cathodes obtained from waste graphite, and graphite interface modification. With the continuous development of related theories and technologies, the research of graphite cathodes will also achieve practical applications.

### 3 Anion-hosting organic cathodes

Organic electrodes (OEs) can be obtained from natural resources or generated from abundant precursors, which makes them promising candidates for low-carbon ESDs [114–116]. OEs can be classified as p-type, n-type, or bipolar electrodes, which can reversibly store anions, cations, or both charge carriers, respectively [117]. Because the anion storage in most p-type organic cathodes operates at moderate potentials within the thermodynamic stability window of electrolytes, electrochemically active organic compounds that are capable of p-type doping and de-doping of anions could be alternatives to graphitic carbon cathodes for DIBs [118]. Organic cathode materials offer other remarkable benefits, including various structural configurations, elemental sustainability, the capacity to tune their characteristics, and several synthesis methods [119,120].

OEs are classified into monomeric molecules and polymers [121]. Because of the absence of an extended conjugated system, monomeric organic molecules are electrically insulating and prone to the dissolution in the electrolyte. Additionally, the tightly packed arrangement of molecules in monomeric organic compounds (for instance, crystalline pyrene, whose intermolecular lengths are insufficient for the diffusion of large anions) renders the anion insertion difficult. By contrast, massive anions can diffuse through flexible and amorphous polymer chains. Important p-type cathodes such as polypyrrole (PPy)-, polyethylenedioxythiophene (PEDOT)-, polyviologen- [122], polyaniline (PANI)- [123], polythiophene (PTh)- [124], dihydrophenazine (Pz)-based polymers [70], porphyrin [125,126], phthalocyanine [127], will be discussed in this section. In addition, we will further discuss the structural properties of the dipolar electrodes, considering that they can store both cations and anions. Based on the research trends, we focus on (1) aromatic amine polymers, (2) heterocyclic polymers, (3) bipolar compounds, and (4) all-carbon-un-saturated compounds (Figure 4).

OEs in DIBs exhibit poor redox activity due to inadequate ionic and/or electronic conductivities [128]. Studies have revealed that adding polar groups to polymer chains and building composite cathodes are two effective methods for improving the redox activity of conjugated polymer cathodes

in DIBs [124,129,130]. This review focuses on the relationship between molecular structure and properties. Therefore, composites with organic molecules and highly conductive materials are not discussed [130].

#### 3.1 Aromatic amine polymers

Aromatic amines exhibit high specific capacity, high ED, good cycle stability, and high rate capabilities in DIBs, which contribute to their exceptional performance, surpassing the performance of the most famous graphite cathode [138]. Aromatic amine polymers provide several advantages, including cost-effectiveness and readily accessible raw materials. When used as cathodes, these polymers exhibit notable characteristics such as elevated redox potentials, substantial specific capacities, and high charge-discharge rates (Table 2). The most notable examples of aromatic amine polymers include polytriphenylamine (PTPA, theoretical specific capacity ( $C_{th}$ ) is  $110 \text{ mAh g}^{-1}$ ), polyaniline (PANI,  $C_{th}$  is  $294 \text{ mAh g}^{-1}$ ), and polydiphenylamine (PDPA,  $C_{th}$  is  $160 \text{ mAh g}^{-1}$ ), all of which have been studied.

##### 3.1.1 PANI

Polyaniline (PANI), a commonly studied conjugated polymer, has attracted considerable attention in energy storage because of its impressive theoretical capacity of  $294 \text{ mAh g}^{-1}$  [139]. The presence of irreversible reactions resulting from the various oxidation states of PANI reduces the actual capacity, which is less than half of the theoretical value [140]. The modification of PANI can improve the anion-hosting properties. For example, the presence of organic chains in doping states leads to the generation of additional “charge islands”. These islands overlap and spread out within the polymers, thereby enhancing the electrical conductivity of conjugated polymers [141]. Jiao *et al* [142] compared the reversible anion-storage capability between pure PANI and protonated PANI (P-PANI). Protonation affects the oxidation-state adjustments of nitrogen atoms on the conjugated backbones of PANI, which exposes additional active sites, resulting in the acquisition of high capacity. The CV curves obtained for P-PANI in a  $1 \text{ mol L}^{-1}$  solution of  $\text{NaClO}_4$  exhibited two sets of redox peaks at  $3.97/3.85$  and  $3.0/2.7 \text{ V}$ . These peaks were ascribed to the coordination and de-coordination of  $\text{ClO}_4^-$  ions with the para-disubstituted benzene ring and quinone diimine groups in P-PANI. The capacity retention of P-PANI was 68%, which is approximately 5 times as high as that of pristine PANI. Furthermore, the performance of P-PANI was evaluated in two electrolytes:  $1 \text{ mol L}^{-1}$   $\text{NaClO}_4$  and  $1 \text{ mol L}^{-1}$   $\text{NaPF}_6$ . A specific capacity of  $210 \text{ mAh g}^{-1}$  was observed for P-PANI in  $1 \text{ mol L}^{-1}$   $\text{NaClO}_4$ , which is higher than the capacity of  $147 \text{ mAh g}^{-1}$  achieved in a  $1 \text{ mol L}^{-1}$   $\text{NaPF}_6$  solution, indicating that P-PANI exhibits excellent compatibility with  $\text{ClO}_4^-$  during

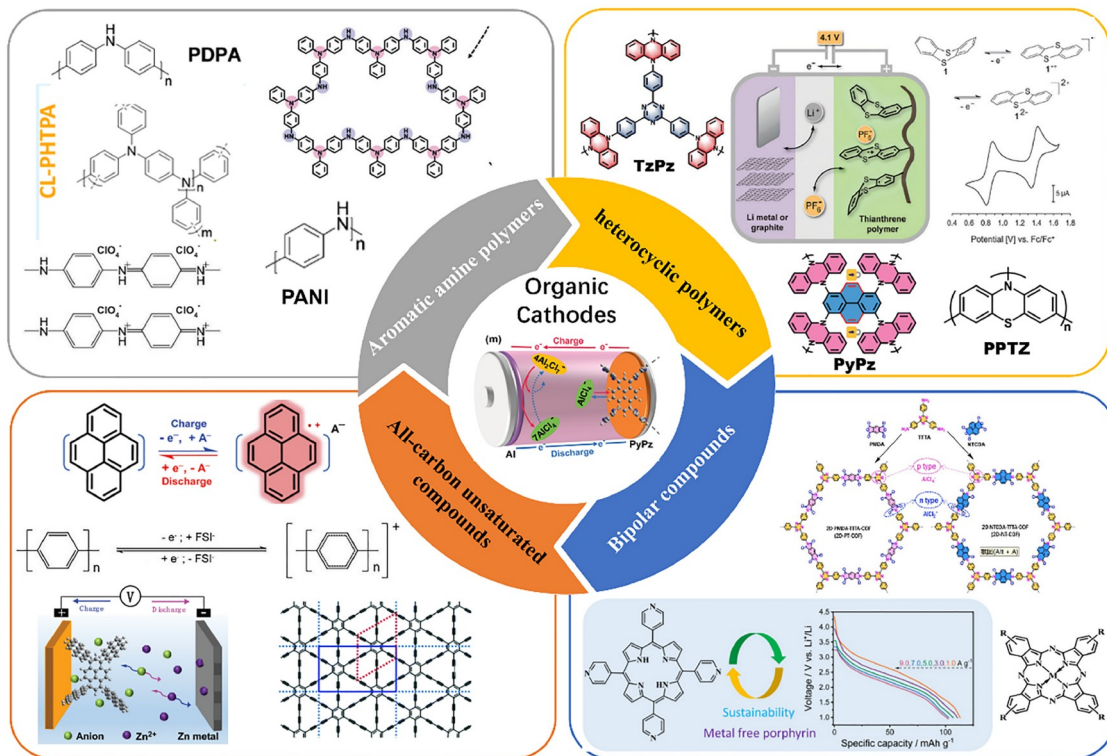


**Figure 4** Organic cathodes for anions hosting aromatic amine polymers, heterocyclic compounds, bipolar polymers, and all-carbon-unsaturated compounds [131–133]. Graph for organic cathodes in the middle. Reproduced with permission [70]. Copyright 2022, Wiley-VCH. Graphs for aromatic amine polymers. Reproduced with permission [123]. Copyright 2021, American Chemical Society. Reproduced with permission [134]. Copyright 2021, Wiley-VCH. Graphs for Heterocyclic polymers. Reproduced with permission [71]. Copyright 2021, Wiley-VCH. Reproduced with permission [70]. Copyright 2022, Wiley-VCH. Reproduced with permission [135]. Copyright 2015, the Royal Society of Chemistry. Graphs for bipolar compounds. Reproduced with permission [127]. Copyright 2019, Wiley-VCH. Reproduced with permission [125]. Copyright 2023, the Royal Society of Chemistry. Graphs for all-carbon-unsaturated compounds. Reproduced with permission [72]. Copyright 2021, the Royal Society of Chemistry. Reproduced with permission [136]. Copyright 2021, American Chemical Society. Reproduced with permission [137]. Copyright 2022, Elsevier (color online).

electrochemical reactions.

Because  $\text{PF}_6^-$  is a class of anions and their reversible storage is critical in DIBs, novel materials based on PANI to reversibly store  $\text{PF}_6^-$  have also developed. Fluorine (F) exhibits electron-withdrawing characteristics, a small van der Waals radius, and low polarizability. Sun *et al.* [143] reported that the incorporation of F into a protonated PANI/CNT composite (FPHC) can enhance the stability of  $\text{PF}_6^-$  storage properties. The incorporation of F can also decrease the energy gap between the highest occupied molecular orbital (HOMO) and the lowest unoccupied molecular orbital (LUMO), enhancing the electrical conductivity. The formation of reversible and stable covalent bonds between  $\text{PF}_6^-$  and FPHC can be attributed to the interaction between F in  $\text{PF}_6^-$  and hydrogen (H) in the  $-\text{NH}-$  group in FPHC. The FPHC cathode could achieve a specific capacity of  $115 \text{ mAh g}^{-1}$  following 200 cycles at a rate of  $0.2 \text{ A g}^{-1}$ . Additionally, the cathode exhibited a consistent and reversible capacity of  $73 \text{ mAh g}^{-1}$  after 2,000 cycles at a rate of  $2 \text{ A g}^{-1}$ . These findings established a strong foundation for the development of advanced DIBs based on modified PANI.

### 3.1.2 PDPA

PDPA, a derivative of PANI, has superior mechanical, electrochemical, and conductivity. The N atoms in PDPA and PANI are located in imine groups ( $-\text{NH}-$ ), which can be doped to improve electrical conductivity [149]. The biphenyl groups that connect the  $-\text{NH}-$  groups in PDPA differ from the monophenyl ring structure of PANI, which has good conjugated conductivity and stabilizes the positive ion center during the anion storage, improving cycle stability [150]. Therefore, PDPA can be used as a highly conductive electrode material by improving the content of active material and reducing the content of conductive additives. In general, electrodes prepared with highly conductive PDPA have active materials of up to 80%, and their electrochemical performance is comparable to that of advanced inorganic cathodes, whereas electrodes prepared with most OEs have conductivities of only 40%–60% [145].

### 3.1.3 PTPA

Although PTPA exhibits a lower theoretical capacity than PANI and PDPA, its cycling performance is excellent because of its quaternary nitrogen intermediate, with improved

**Table 2** Electrochemical performance comparison of various cathodes based on aromatic amine polymers.

	Cathode	Anion	Voltage	Specific capacity@current rate	Cycling capability
Al-DIB	PTh/MWCNT [124]	AlCl <sub>4</sub> <sup>-</sup>	0–2.2 V	216 mAh g <sup>-1</sup> @1/20 C	300 cycles@1/5 C
Mg-DIB	PANI [144]	NO <sub>3</sub> <sup>-</sup>	0–1.5 V	0.071 mAh cm <sup>-2</sup> @0.2 mA cm <sup>-2</sup> 0.041 mAh cm <sup>-2</sup> @20 mA cm <sup>-2</sup>	81.5% after 3,500 cycles@5 mA cm <sup>-2</sup>
Na-DIB	P-PANI [142]	ClO <sub>4</sub> <sup>-</sup>	2.5–4.2 V	210 mAh g <sup>-1</sup> @0.2 A g <sup>-1</sup> 123 mAh g <sup>-1</sup> @3 A g <sup>-1</sup>	103 mAh g <sup>-1</sup> for 2,000 cycles@2 A g <sup>-1</sup>
Na-DIB	FPHC [143]	PF <sub>6</sub> <sup>-</sup>	2.2–4.2 V	116 mAh g <sup>-1</sup> @0.2 A g <sup>-1</sup> 78 mAh g <sup>-1</sup> @3 A g <sup>-1</sup>	115 mAh g <sup>-1</sup> after 200 cycles@0.2 A g <sup>-1</sup> , 73 mAh g <sup>-1</sup> after 2,000 cycles@2 A g <sup>-1</sup>
Li-DIB	PDPA [145]	PF <sub>6</sub> <sup>-</sup>	2.5–4.2 V	116, 127 and 126 mAh g <sup>-1</sup> @ 0.1 A g <sup>-1</sup> with 50%, 70% and 80% active materials	91%, 81% and 79% for 100 cycles @0.1 A g <sup>-1</sup> with 50%, 70% and 80% of active material
K-DIB	PDPA [145]	PF <sub>6</sub> <sup>-</sup>	2.5–4.5 V	120 mAh g <sup>-1</sup> @0.1 A g <sup>-1</sup>	58% after 100 cycles@0.1 A g <sup>-1</sup>
Ca-DIB	PTPA [146]	TFSI <sup>-</sup>	3.8 V (vs. Ca/Ca <sup>2+</sup> ) 2.45 V (graphite anode)	88 mAh g <sup>-1</sup> @0.1 A g <sup>-1</sup> 86, 85, 77 and 55 mAh g <sup>-1</sup> @2, 3, 5 and 10 A g <sup>-1</sup>	82% after 2,000 cycles@5 A g <sup>-1</sup>
Mg-DIB	PTPA@graphene nano- plates (PTGNP) [147]	B(hfip) <sub>4</sub> <sup>-</sup>	3.4–2.5 V (Mg anode) average operating voltage of ~3 V	105 mAh g <sup>-1</sup> @10 <sup>th</sup> cycle 94 mAh g <sup>-1</sup> @10 C	57% after 500 cycles@10 C
Ca-DIB	PTGNP [147]	B(hfip) <sub>4</sub> <sup>-</sup>	3.7–3.2 V, ~3.5 V (Ca anode) 3.5 to 2.3 V, ~2.8 V (CaSn <sub>3</sub> anode)	85 mAh g <sup>-1</sup> @5 <sup>th</sup> cycle @10 C	60% after 3,000 cycles@10 C
Li-DIB	CL-PHTPA [123]	PF <sub>6</sub> <sup>-</sup>	2.5–4.2 V	112.5, 102.6, and 81.1 mAh g <sup>-1</sup> @0.1, 1, and 10 A g <sup>-1</sup>	98% and 36% after 100 and 15,000 cycles@10 A g <sup>-1</sup>
Zn-DIB	PTPA-based COF [134]	Cl <sup>-</sup>	1.4 V	210.7 mAh g <sup>-1</sup> @0.5 A g <sup>-1</sup> 107.5 mAh g <sup>-1</sup> @6 A g <sup>-1</sup>	87.6% after 1,000 cycles
Li-DIB	Spiro-TAD [148]	ClO <sub>4</sub> <sup>-</sup>	3.6 V	109 mAh g <sup>-1</sup> @50 mA g <sup>-1</sup> 60 mAh g <sup>-1</sup> @2,000 mA g <sup>-1</sup>	98.4% after 1,400 cycles@500 mA g <sup>-1</sup>

stability when storing anions. Furthermore, PTPA exhibits high potential and rapid kinetics. By contrast, the combination of a PTPA cathode with a viable metallic anode can integrate the advantages of both electrodes in relation to ED, cost, and safety.

PTPA demonstrated the potential for constructing dependable Ca-DIBs in both organic and aqueous electrolytes [146]. The reaction mechanism of PTPA involved the reversible association and dissociation of anions with the carbon–nitrogen (C–N) bond, leading to a specific capacity of 88 mAh g<sup>-1</sup> and an average discharge voltage of 3.8 V (vs. Ca/Ca<sup>2+</sup>). When coupled with a graphite anode, the graphite||PTPA full cell exhibits a satisfactory voltage of 2.45 V. The observed behavior demonstrates exceptional stability, as it endures more than 2,000 cycles when maintaining rapid kinetics at a rate of up to 50 C (1 C = 0.1 A g<sup>-1</sup>). The use of a PTPA composite cathode can exhibit reversible storage capabilities for *tetrakis(hexafluoroisopropoxy)* borate [B(hfip)<sub>4</sub>] anions [147]. The cells composed of Mg and Ca demonstrate a voltage exceeding 3 V, a notable PD of approximately 3,000 W kg<sup>-1</sup>, and a substantial ED of approximately 300 Wh kg<sup>-1</sup>.

PTPA-based polymers exhibit excellent electrochemical characteristics. However, the molecular structure of these polymers typically leads to the formation of agglomerated

and intertwined chains, which restrict the ability of their active sites to effectively react with larger anions. This problem may be solved by adopting a simple strategy such as cross-linking, which can yield comparable outcomes to the development of novel and intricate materials. NPDPA and PHTPA precursor polymers were oxidatively polymerized to create cross-linked (CL) materials, CL-NPDPA and CL-PHTPA. (Figure 5a) [123]. The CL-PHTPA material exhibited specific capacities of 112.5, 102.6, and 81.1 mAh g<sup>-1</sup> at current densities of 0.1, 1, and 10 A g<sup>-1</sup>, respectively. Combined with the high capacity retention of CL-PHTPA, this material is promising in satisfactory capacities, remarkable rate capabilities, and acceptable cycling stability.

Designing and preparing a porous PTPA-based conjugated microporous polymer (CMP) cathode can circumvent the problem of low utilization of reactive sites in PTPA. The CMP cathode can effectively accommodate Cl<sup>-</sup> through its pseudocapacitive behavior, rendering CMP suitable for energy storage purposes (Figure 5b) [134]. The three-dimensional structure of the covalent-organic-framework-like conjugated network provides better accessibility to N active sites, resulting in an efficiency of up to 83.2% at a current density of 0.5 A g<sup>-1</sup>. Additionally, CMP exhibited excellent physicochemical stability, with a capacity retention of 87.6% after 1,000 cycles. The use of a highly durable CMP elec-

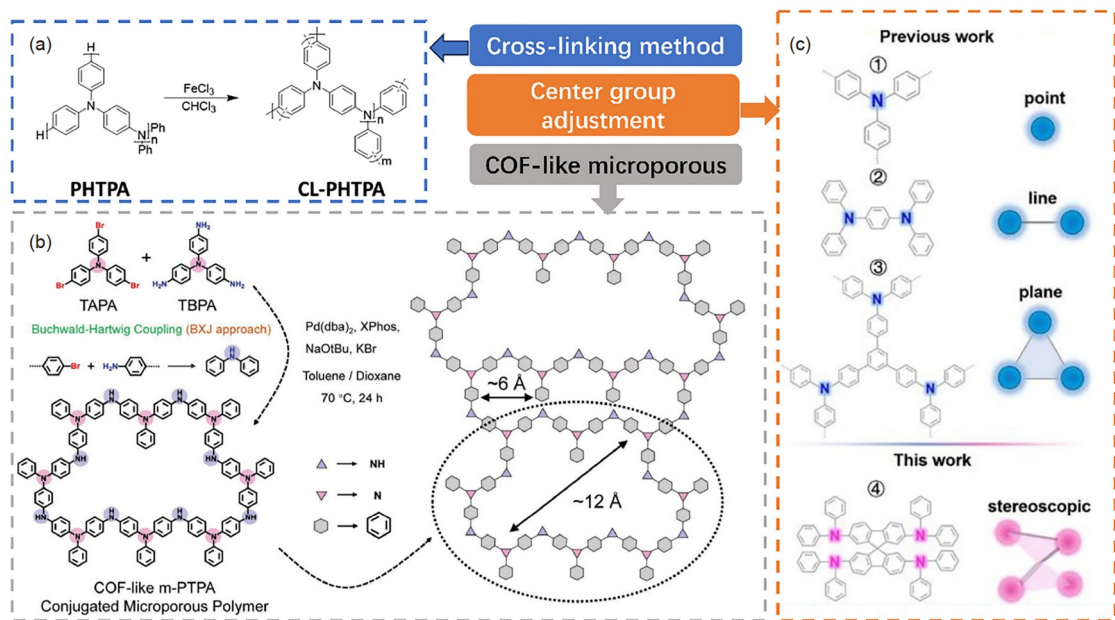


**Figure 5** (a) Cross-linking modification of PHTPA. Reproduced with permission [123]. Copyright 2021, American Chemical Society. (b) Schematic of the synthesis route of COF-like polytriphenylamine CMP and its structure. Reproduced with permission [134]. Copyright 2021, Wiley-VCH. (c) Molecular structures of triphenylamine-based compounds. Reproduced with permission [148]. Copyright 2023, Elsevier (color online).

trode in the construction of a Zn-DIB resulted in an impressive ED of 236 Wh kg<sup>-1</sup> and a PD of 6.8 kW kg<sup>-1</sup>. The findings laid a foundation for the systematic development of PTPA-based sophisticated cathodes for high-energy applications.

Another solution is to design and prepare molecules with rigid spirofluorene structure, specifically 2,20,7,70-tetrakis-(diphenylamine)-9,90-spirobifluorene (Spiro-TAD) (Figure 5c) [148]. The Spiro-TAD exhibits an inherently steric structure that renders it favorable chemical stability and considerable internal volume, facilitating the rapid diffusion kinetics of anions within the organic electrolyte. Consequently, the Spiro-TAD electrode exhibits notable insolubility and reduced steric hindrance, resulting in a substantial actual capacity of 109 mAh g<sup>-1</sup> (with an approximate utilization ratio of active groups at 100%) at 50 mA g<sup>-1</sup>. Moreover, the electrode demonstrates a high discharge voltage of 3.6 V (compared with Li<sup>+</sup>/Li), exceptional rate capability (achieving 60 mAh g<sup>-1</sup> at a current density of 2,000 mA g<sup>-1</sup>), and remarkably stable cycling performance (retaining 98.4% of its capacity after 1,400 cycles at a current density of 500 mA g<sup>-1</sup>) in half cells. The excellent electrochemical performance of the system can be attributed to the strong and efficient adsorption/desorption of  $\text{ClO}_4^-$  anions. Furthermore, a Li-DIB with all-organic components (referred to as a-OLDIBs) is fabricated using Spiro-TAD as the cathode material and 3,4,9,10-perylenetetracarboxylic diimide (PTCDI) as the anode material. This battery exhibited excellent long-term cycling performance, maintaining a capacity of 87.5 mAh g<sup>-1</sup> even after under-

going 800 charging-discharging cycles. The study offered insights into advancements in entirely organic battery system design.

To sum up, aromatic amine polymers are a critical class of organic anion-hosting materials. Although PANI exhibits a high theoretical capacity, its cycle performance should be improved, and despite the theoretical capacity of PTPA not being high, it exhibits excellent conductivity and can stabilize the quaternary nitrogen positive ion intermediate during the anion storage, which improves its cycle stability and rate performance. Obtaining PTPA with high capacity through structural design is a critical topic of research. By contrast, considering the easy synthesis and low cost of PANI, obtaining PANI with excellent cycling performance and rate performance can be a critical research hotspot.

### 3.2 Heterocyclic polymers

Heterocyclic aromatic hydrocarbons containing nitrogen, oxygen and/or sulfur atoms have been extensively studied as redox-active groups. Heterocyclic polymers encompass a class of heterocyclic monomers incorporated into polymers and the heterocyclic monomers containing thianthrene, phenazine (Pz), phenothiazine (PTZ), and phenoxazine functional groups. They have the following characteristics: (1) high working potential: for example, thianthrene has the anion reaction potential of 4.09 V vs. Li/Li<sup>+</sup>, which is higher than traditional cathodes in LIBs, such as LiCoO<sub>2</sub> and LiFePO<sub>4</sub> [135]; (2) cathodes based on heterocyclic polymers exhibit high cycling stability and reversible capacity: be-

cause of efficient positive charge delocalization in the conjugated structure, the skeleton of the dihydropheophazine (DPZ) unit did not alter. According to the Hückel's rule, oxidation changes the electrons of DPZ peripheral from  $4n$  to  $4n+2$ , rendering the corresponding dihydropheophazine cation stable.

Based on the described heterocyclic polymers, the anion storage process can be explained as follows: upon charging, the redox-active sites are oxidized, resulting in the accumulation of positive charges. Anions, such as  $\text{PF}_6^-$ , derived from LiPF<sub>6</sub>-based electrolytes are inserted into the structure of the polymer, leading to charge balancing and the desired effect. Electrolyte cations react with the anode electrode with a similar mechanism in LIBs.

Similar to all organic electrode materials, small molecules or dimer heterocyclic materials have certain solubility and poor conductivity, resulting in poor electrochemical performance. For instance, small molecular *N,N'*-substituted phenazine (NSPZ) cathodes, initially established by Lee and Kang *et al.* [151], entail a reversible two-electron redox reaction in Li-DIBs. However, the specific capacity and the cycle life of small molecular NSPZ are unsatisfactory because of the dissolution of active material in organic electrolytes. The dimerization strategy can partially suppress the dissolution of molecules and improve cycling stability. This phenomenon opens novel avenues for the development of polymerized cathodes. Heterocyclic active units can be

suspended as pendants on a durable polymer chain, either in a linear arrangement or through the cross-linking *via* cross-coupling reactions. Additionally, these units can undergo copolymerization with other p-type units.

Most polymer cathodes reported so far exhibit limitations such as diminished redox activity, sluggish kinetics, and limited cycling durability. Therefore, we summarize the design concepts of polymer cathodes based on heterocyclic active units (Table 3). In this section, we comprehensively describe the relationship between electrochemical performance and the molecular structures with heterocyclic compounds as (1) the side chain of polymers and (2) the primary chain of polymers.

### 3.2.1 Polymers with heterocyclic compounds as side chain groups

To prevent the dissolution of electrode materials, heterocyclic compounds are functionalized as redox-active side groups in the aliphatic polymer chains. Such compounds have been used in TEMPO-based OEs [157]. Subsequently, researchers examined the potential of thianthrene-functionalized polynorbornenes as cathode materials with high voltage capabilities in DIBs [135].

Achieving high cycling stabilities for more than 1,000 cycles is challenging because the electrode material or electrolyte constantly undergoes deterioration. A concept for redox polymers as cathode materials involving  $\pi-\pi$  interac-

**Table 3** Electrochemical performance comparison of various cathodes based on heterocyclic polymers

	Cathode	Anode	Voltage	Specific capacity	Cycling capability
Li-DIB	X-PVAPT [152]	Li metal	3.2–3.8 V	81 mAh g <sup>-1</sup> @1 C 69 mAh g <sup>-1</sup> @100 C	86% for 10,000 cycles @100 C
Li-DIB	TzPz [71]	Li metal	3.22/3.11, 3.95/3.86 V	192 mAh g <sup>-1</sup> @0.2 A g <sup>-1</sup> 108 mAh g <sup>-1</sup> @30 A g <sup>-1</sup>	10,000 cycles @5 A g <sup>-1</sup>
Al-DIB	PyPz [70]	Al metal	~ 0.89 V	231 mAh g <sup>-1</sup> @0.1 A g <sup>-1</sup> 116 mAh g <sup>-1</sup> @30 A g <sup>-1</sup>	78.1% for 100,000 cycles @10 A g <sup>-1</sup>
Li-DIB	PDPAPZ [153]	Li metal	3.5–3.6 V	101 mAh g <sup>-1</sup> @5 A g <sup>-1</sup> 82 mAh g <sup>-1</sup> @20 A g <sup>-1</sup>	86% for 100 cycles @5 A g <sup>-1</sup> 34% for 25,000 cycles @5 A g <sup>-1</sup>
Li-DIB	Thianthrene-functionalized polynorbornenes [135]	/	4.1 V	66 mAh g <sup>-1</sup> @1 C	30% for 100 cycles
Li-DIB	PPTZ [132]	/	2.5–4.3 V, 3.5 V	157 mAh g <sup>-1</sup> @50 mA g <sup>-1</sup> 100 mAh g <sup>-1</sup> @1,000 mA g <sup>-1</sup>	77% for 500 cycles @200 mA g <sup>-1</sup>
Al-DIB	PVBPX [154]	/	1.0 V and 1.7 V	126, 119, 113, 110, 100, 90, 78, 60 mAh g <sup>-1</sup> @0.3, 0.5, 0.8, 1, 2, 3, 5, 10, 0.2 A g <sup>-1</sup>	88 mAh g <sup>-1</sup> after 5,000 cycles @5 A g <sup>-1</sup>
Na-DIB	BPyPz [155]	Na metal	1.5 to 4.3 V	205 mAh g <sup>-1</sup> @0.5 C 205, 195, 177, 169, 155, 149, 144 and 126 mAh g <sup>-1</sup> @0.5, 1, 2, 5, 8, 10 and 20 C	89% for 300 cycles @0.5 C
Na-DIB	TPyPz [155]	Na metal	1.5 to 4.3 V	178, 128, 95, 87, 84, 75 and 66 mAh g <sup>-1</sup> @0.5, 1, 2, 5, 8, 10 and 20 C	/
Mg-DIB	x-PVCz [156]	Mg	3.15 V	122 mAh g <sup>-1</sup> @2,000 mA g <sup>-1</sup>	94.2% for 2,000 cycles @1,500 mA g <sup>-1</sup>
Mg-DIB	x-PVCz [156]	3Mg/Mg <sub>2</sub> Sn	2.93 V	133 mAh g <sup>-1</sup> to 131, 129, 125, 123, and 121 mAh g <sup>-1</sup> @100, 200, 500, 1,000, 1,500 and 2,000 mA g <sup>-1</sup>	97.3% for 1,000 cycles @1,100 mA g <sup>-1</sup>

tions between redox-active groups has been proposed [158]. This interaction increases the cycle stability and charge transport channels, leading to high electron-transfer rates and rate capability. Poly(3-vinyl-*N*-methylphenothiazine) (PVMPT) was used as a cathode-active material in a Li-organic battery to showcase the idea. PVMPT-based composite cells had outstanding cycling stability and high rate capability, retaining 93% of the original capacity after 10,000 cycles at 10 C and 52% at 100 C.

A phenoxazine-polymer-based p-type positive electrode known as poly(vinylbenzyl-*N*-phenoxazine) (PVBX) was used in batteries [154]. The specific capacity of 133 mAh g<sup>-1</sup> in the PVBX could be attributed to the presence of dual active sites, namely N and O. Furthermore, the incorporation of dual active sites onto a polymer matrix effectively mitigated the dissolution process in the electrolyte solution. The insolubility of PVBX, combined with its extended  $\pi$ -conjugated system and anionic redox chemistry without the bond rearrangement, facilitated rapid kinetics and contributed to an impressive ultralong lifetime of 50,000 cycles. This study provided valuable insights for designing cathodes suitable for advanced energy storage systems (EESs) on a large scale.

### 3.2.2 Heterocyclic polymers with cross-linking strategy

Cross-linking (CL) between the active units produced considerably increases the porosity and surface area, allowing anions to diffuse readily and maintain the dimensionality of the material during the charge-discharge process. Esser and collaborators [159] synthesized two polymers by incorporating phenoxazine into a linear poly(3-vinyl-*N*-methylphenoxazine) (PVMPO) and a CL poly-(vinylene) (X-PVMPO). CL X-PVMPO outperformed linear PVMPO in cycle stability and rate performance. At 100 C, X-PVMPO exhibited gradual capacity deterioration over 10,000 cycles with 74% capacity retention.

The incorporation of heterocyclic active units in polymers results in the stabilization of the charged state, while decreasing attainable specific capacities. Desmaizieres *et al.* [152] revealed that the incorporation of anisyl substituents considerably influenced the electrochemical performance of aliphatic PTZ polymers. Derivatives of poly(styrene), PSAPT (poly(styrylanisylphenothiazine)), and PSAPT-X-DVB (divinylbenzene cross-linked PSAPT) exhibit the interactions, which are typical PTZ-based redox polymers. Although their specific capacities are low, these materials exhibit improved cycle stabilities. Due to a dissolution/re-deposition process, PVAPT has lower capacity but has improved cycle stability. After 10,000 cycles at 100 C, CL X-PVAPT has remarkable cycling stabilities and rate performance, preserving 86% of the capacity. These results imply that molecular structural modifications can be used to modify OEs. Cross-linking low-molecular-weight PVCz

produces x-PVCz, which improves the electronic conductivity and micro-to-macro pore density, achieving near-theoretical capacities (122 mAh g<sup>-1</sup>) and minimal voltage drop at 2,000 mA g<sup>-1</sup> (14.3 C) in Mg-DIBs [156]. This study demonstrated the high quality of x-PVCz, revealing the potential utility of cross-linking in the development of functional anion hosts.

### 3.2.3 Polymers with heterocyclic compounds as main chain

A marked decrease in the theoretical capacity in the designed structure can be attributed to the presence of inactive moieties. To fully use the benefits of the heterocyclic unit, undertaking the development of innovative heterocyclic-based polymers that possess simpler structures, higher theoretical capacities, and easier synthesis methods is imperative. The structure of the heterocyclic unit as the main chain can increase the mass of the active substance to a certain extent compared with the side chain.

The p-type polymer polyphenothiazine (PPTZ) can be produced from PTZ in the oxidation reaction [132]. PPTZ, a polymer with cross-linked structures, shows improved electrochemical performance (high capacity of 157 mAh g<sup>-1</sup>, high capacity retention of 77% for 500 cycles, and a stable discharge voltage) in rechargeable Li-DIBs. The redox mechanism of PPTZ was studied through a comprehensive approach involving electrochemical analysis, *ex-situ* FTIR spectra, and XPS, as well as DFT calculations (Figure 6). The investigation revealed a completely reversible one-electron reaction, with the N atom as the active center. Furthermore, the study highlighted the difficulty in facilitating the subsequent one-electron reaction, providing novel perspectives on the design and synthesis of p-type polymers by using electroactive N-heteroaromatic units. The simple configuration and convenient synthesis of p-type polymers may result in favorable electrochemical performance, which is crucial for the viable implementation of these materials in economically efficient DIBs.

The polymerization of *N,N'*-diphenyl-5,10-dihydrophenothiazine (denoted as p-DPPZ) can considerably reduce solubility and avoid the internal shuttle effect, which can be harmful to the electrochemical performance. By substituting the benzene ring with various functional groups, electron-transfer kinetics can be improved [160]. The p-DPPZ cathodes in K-DIBs demonstrated an excellent specific capacity of 162 mAh g<sup>-1</sup> when subjected to a current density of 200 mA g<sup>-1</sup>. These cathodes exhibited excellent performance at high current densities in the range 2–10 A g<sup>-1</sup>, allowing for the rapid charge and discharge time of approximately 1–4 min. Furthermore, they maintained a specific capacity of 125–145 mAh g<sup>-1</sup> with retention rates of 96% and 79% after 100 and 1,000 charging-discharging cycles, respectively [161].

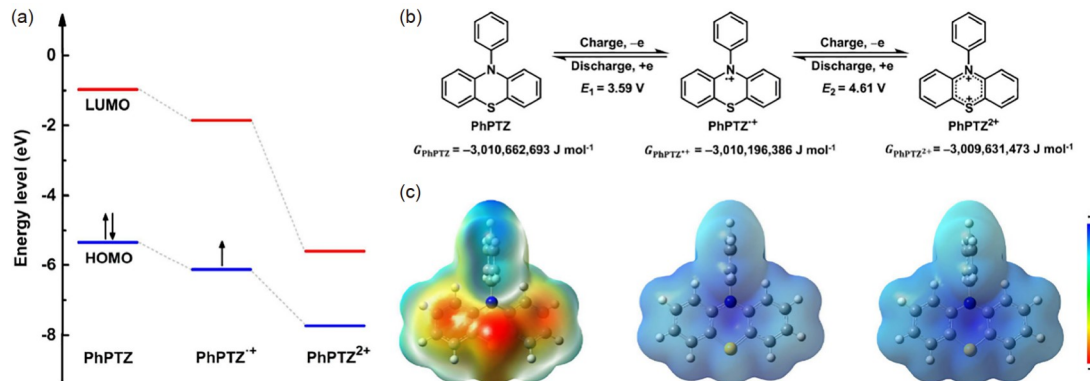


**Figure 6** Electrochemical redox mechanism and DFT calculation results of the electroactive unit (PhPTZ) of PPTZ. (a) Calculated LUMO-HOMO energy levels of PhPTZ and its oxidation products, including radical cation ( $\text{PhPTZ}^+$ , spin up) and divalent cation ( $\text{PhPTZ}^{2+}$ ); (b) two-step electrochemical redox reaction from PhPTZ to  $\text{PhPTZ}^{2+}$  and calculated oxidation potentials; (c) calculated electrostatic potential (ESP) maps of the three molecules. Reproduced with permission [132]. Copyright 2021, Wiley-VCH (color online).

The polymerization of various active units can be used as efficient electrode materials. Two distinct copolymers, namely dihydrophenazine with diphenylamine (PDPAPZ) and phenothiazine (PPTZPZ), were synthesized and subsequently examined as potential cathode materials for DIBs [153]. The PDPAPZ||Li cells exhibited notable rate capability, achieving specific capacities of 101 and 82 mAh g<sup>-1</sup> at current densities of 5 and 20 A g<sup>-1</sup> within the potential range of 3.5–3.6 V, respectively. The batteries exhibited satisfactory operational stability, as indicated by their capacity retention rates of 86% and 34% after 100 and 25,000 cycles, respectively. Potassium PDPAPZ||K cells demonstrated a notable ED of 398 Wh kg<sup>-1</sup>. These results demonstrated that PDPAPZ exhibits comparable performance to leading organic cathode materials in terms of its suitability for high-rate lithium and potassium batteries.

**3.2.4 Rigid flexible adjustment of heterocyclic polymers**  
The modulation of polymer chain flexibility can affect the diffusion characteristics of ions inside polymeric materials, and the ionic diffusion coefficient can be increased by introducing a suitable twisted group to disrupt the stiff polymer backbone. Polymers with more flexible chains demonstrate higher galvanometric and volumetric power/energy densities, despite their reduced surface area and electrical conductivity, compared with the polymers with a more rigid chain structure (Figure 7a). This approach may be advantageous in the development of polymeric battery materials with a high PD while maintaining their volumetric ED. For instance, Zhang and Zhao *et al.* [162] designed and synthesized three polymers based on redox-active DPPZ with different chain rigidities (Figure 7b): DPPZ spanned by  $-\text{CH}_2-$  (name it as *p*-DPPZR1),  $-\text{CH}=\text{CH}-$  (the *trans*-isomer, name it as *p*-DPPZR2), and  $-\text{C}\equiv\text{C}-$  (name it as *p*-DPPZR3). Each of the three polymers had a different degree of chain flexibility (Figure 7c). The diffusion coefficients of the three

polymers exhibited similar trends in their variations during charging and discharging. These findings provide the evidence for the impact of chain stiffness on the diffusivity. Compared with *p*-DPPZR2 and *p*-DPPZR3, respectively, the chemical diffusion coefficient of  $\text{PF}_6^-$  in *p*-DPPZR1 was found to range from  $10^{-10}$  to  $10^{-12}$  cm<sup>2</sup> s<sup>-1</sup>, demonstrating an approximate increase in magnitude by 2–3 orders.

Polymeric alkyl viologens such as poly(butyl viologen dichloride) (PBV-Cl<sub>2</sub>) [122] and poly(hexyl viologen dichloride) (PHV-Cl) are a crucial class of rigid-flexible polymers, which have a large specific surface area and an excellent ability to stabilize anions [163]. For example, PBV-Cl<sub>2</sub> [122], as the cathode material of Li–PBV-Cl<sub>2</sub> DIB, demonstrated the highest actual ED of 470 Wh kg<sup>-1</sup>, attributable to the PBV-Cl<sub>2</sub> cathode's superior reversible capacity of 183 mAh g<sup>-1</sup>. The addition of the fluoroethylene carbonate (FEC) to the electrolyte to enhance the compatibility with the Li anode resulted in considerable improvements in both cycling stability (88% after 300 cycles) and rate capability (75% at 5,000 mA g<sup>-1</sup>). When combined with a magnesium anode, PHV-Cl exhibited cathodic behavior through reversible anion deinsertion/insertion [164]. Furthermore, the electrochemical characteristics of PHV-Cl are not influenced by specific electrolytes. Although the charge balancing of anionic species may vary, their amorphous nature enables them to exhibit similar electrochemical properties. The compound PHV-Cl exhibits a notable capacity of 171 mAh g<sup>-1</sup> at an average discharge potential of 1.33 V, leading to a considerably high ED of 227 Wh kg<sup>-1</sup>.

### 3.2.5 Microporous and donor–acceptor structural design of heterocyclic polymers

Most polymer cathodes based on heterocyclic polymers that have been reported continue to exhibit limitations such as diminished redox activity, sluggish kinetics, and limited cycling durability.

As described in Section 3.1.3, the CMP materials possess porous structure and high surface area, thus can effectively increase the specific capacity of DIBs because their porosity can increase the utilization rate of active sites. Two CMPs, namely PyPz and PhPz, were developed by coupling the redox-active dihydrophenazine (Pz) with pyrene (Py) or biphenyl (Ph) (Figure 8a). These polymers can be used as cathodes for Al-DIBs and can host  $\text{AlCl}_4^-$  ions [70]. PyPz shows a higher surface area of  $635 \text{ m}^2 \text{ g}^{-1}$  than PhPz ( $163 \text{ m}^2 \text{ g}^{-1}$ ), and a more favorable hierarchical porous structure combining micropores with mesopores. Consequently, PyPz exhibited enhanced redox activity compared with PhPz. Therefore, the PyPz cathode exhibited a considerably greater capacity of  $231 \text{ mAh g}^{-1}$  than the PhPz cathode, which exhibited a capacity of  $137 \text{ mAh g}^{-1}$ . The superior rate performance and exceptional cyclability of PyPz can be attributed to its porous structure and insolubility, which enable it to withstand over 100,000 cycles without undergoing the degradation. Furthermore, the rapid kinetics exhibited by PyPz in storing  $\text{AlCl}_4^-$  enables its effective performance at both low temperature ( $-30^\circ\text{C}$ ) and a high

areal capacity of  $2.53 \text{ mAh cm}^{-2}$ . These results indicated that redox-active conjugated polymers possess considerable potential as advanced organic cathodes for sustainable aqueous DIBs (Figure 8b). The electrochemical performance of these cathodes can be improved through deliberate structural design.

By combining the electron-donating and the electron-withdrawing units into a polymer heterocyclic chain, a donor–acceptor (D–A)-conjugated microporous polymer configuration was obtained, which exhibited an increased degree of polymer conjugation and a reduced band gap of the polymer, thereby promoting the efficient transport of electrons along polymer chains. For instance, the cathode composed of TzPz (Figure 9) from electron-donating Pz and electron-withdrawing 2,4,6-triphenyl-1,3,5-triazine (Tz) in a DIB exhibited a notable reversible capacity of  $192 \text{ mAh g}^{-1}$  at a current density of  $0.2 \text{ A g}^{-1}$ , demonstrating exceptional rate performance with a capacity of  $108 \text{ mAh g}^{-1}$  at a current density of  $30 \text{ A g}^{-1}$ . The TzPz cathode exhibited a prolonged and consistent cyclability exceeding 10,000 cycles. These findings indicated that the D–A structural design is an ef-

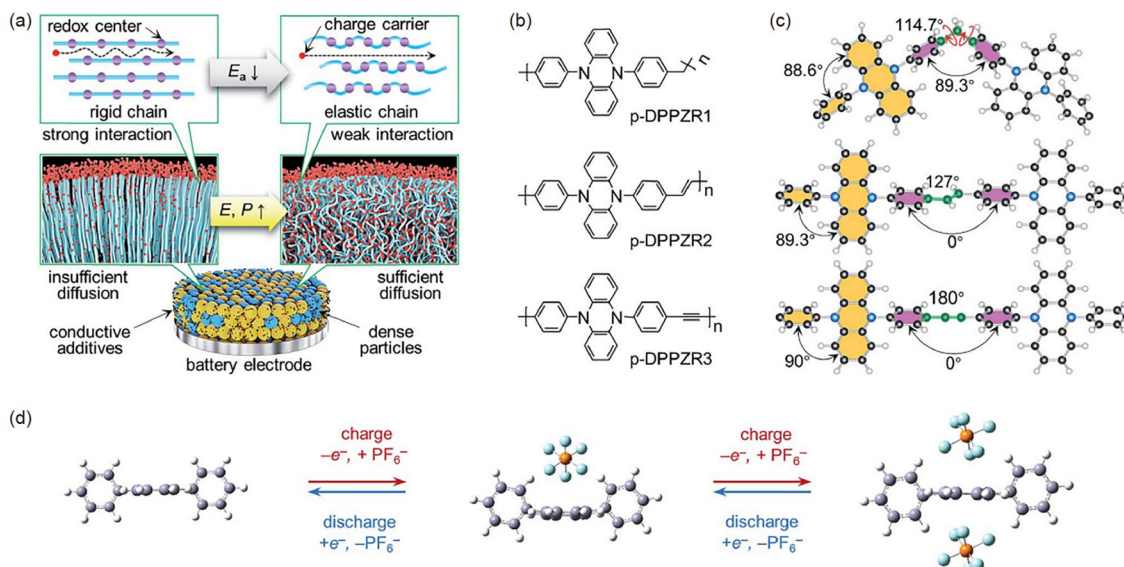


**Figure 7** Structure and properties of *p*-DPPZR1, *p*-DPPZR2 and *p*-DPPZR3. (a) Schematic demonstration of enhancing the power density by decreasing the rigidity of polymer chains. (b) Proposed polymers with variable chain rigidity based on DPPZ. (c) Optimized and other possible chain configurations of DPPZ. (d) Redox mechanism of DPPZ. Reproduced with permission [162]. Copyright 2019, the Royal Society of Chemistry (color online).

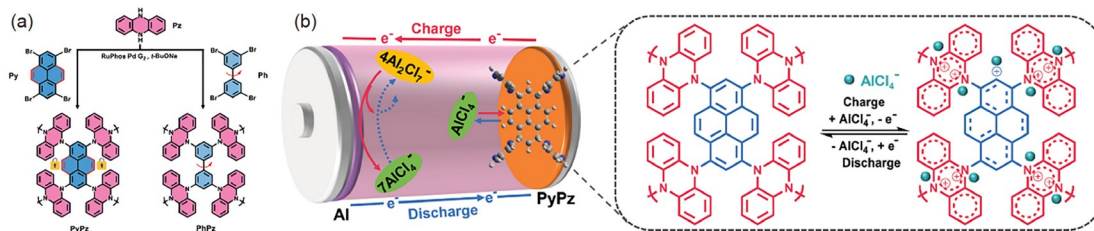


**Figure 8** (a) Synthesis process and the structure of PyPz and PhPz; (b) anion-hosting mechanism of the PyPz cathode. Reproduced with permission [70]. Copyright 2022, Wiley-VCH (color online).

fective approach for the development of polymer cathodes with superior performance for DIBs [71].

Combining the electron-donating 5,10-dihydrophenazine with the electron-withdrawing pyridine derivatives [155] yielded two p-type cathodes with high  $C_{th}$ , namely BPYpZ ( $C_{th}$  is 206 mAh g<sup>-1</sup>) and TPYpZ ( $C_{th}$  is 238 mAh g<sup>-1</sup>) (Figure 10a). The redox potential and electrochemical properties of the materials were considerably influenced by the positioning of the pyridine group, thereby affecting the active site on Pz. The relationship between the structure and property was determined through DFT calculations and a range of electrochemical tests (Figure 10b, 10c). BPYpZ, featuring a pyridine moiety attached to dihydrophenazine at the 2,5-position, exhibited notable reversible specific capacities of 205 mAh g<sup>-1</sup> in half cells and 162 mAh g<sup>-1</sup> in full cells. Conversely, TPYpZ exhibited a densely packed molecular configuration, leading to significant charge repulsion and posing challenges for the reaction of large-size anions, which limited the use of active sites. However, the pre-

paration conditions of D-A type cathodes in the current literature are harsh, and its raw material 5,10-dihydrophenazine is expensive, resulting in a high overall cost. Therefore, D-A type cathodes with excellent performance and low cost need to be further researched and developed.

To synthesize high-performance heterocyclic polymer cathode materials, the research has employed the following strategies (Figure 11): (a) heterocyclic compounds as side chain groups in polymers; (b) cross-linking strategy; (c) heterocyclic compounds as the main chain of polymers; (d) rigid flexible adjustment of heterocyclic polymers and (e, f) microporous and donor–acceptor structural design. These design ideas are aimed at obtaining cathode materials with a higher specific capacity, cycle life, rate performance, and low cost due to simple and inexpensive synthesis methods for studying the relationship between organic electrode structure and performance. In-depth research in the future may facilitate the development of high-performance materials.

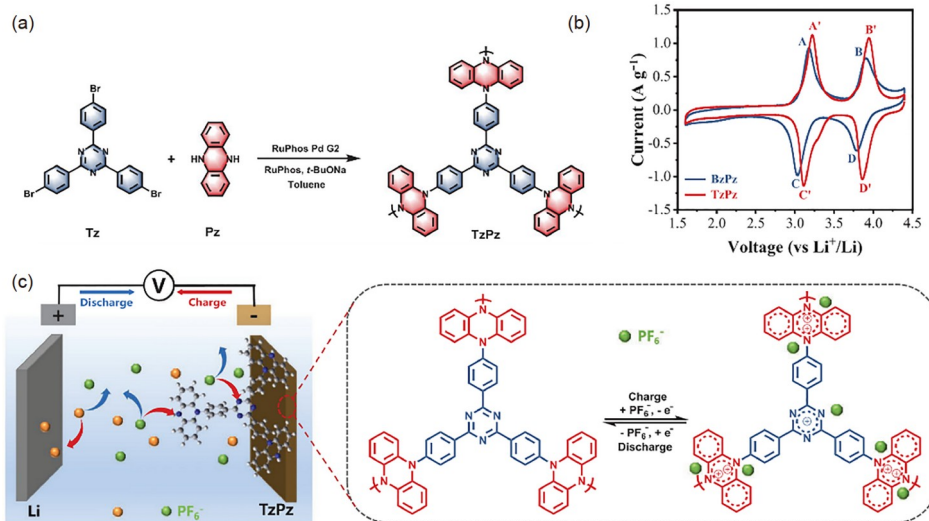


**Figure 9** (a) Synthesis route for TzPz with notional polymer structures. (b) CV curves of the BzPz and TzPz cathodes at 1 mV s<sup>-1</sup>. (c) Schematics of the electrochemical reaction mechanism of the TzPz-based cathode. Reproduced with permission [71]. Copyright 2021, Wiley-VCH (color online).

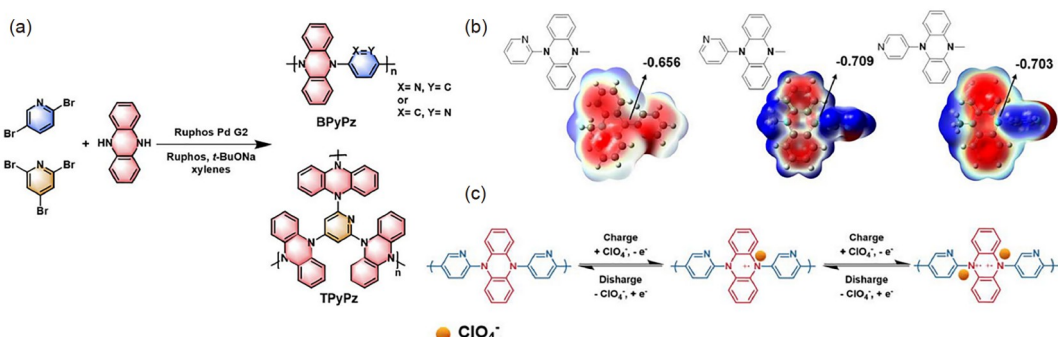


**Figure 10** (a) Synthesis routes for BPYpZ and TPYpZ. (b) Calculated ESP and Mulliken charge distribution on the van der Waals surface of o-Pz, m-Pz and p-Pz. (c) The anion storage mechanism of BPYpZ. Reproduced with permission [155]. Copyright 2023, the Royal Society of Chemistry (color online).

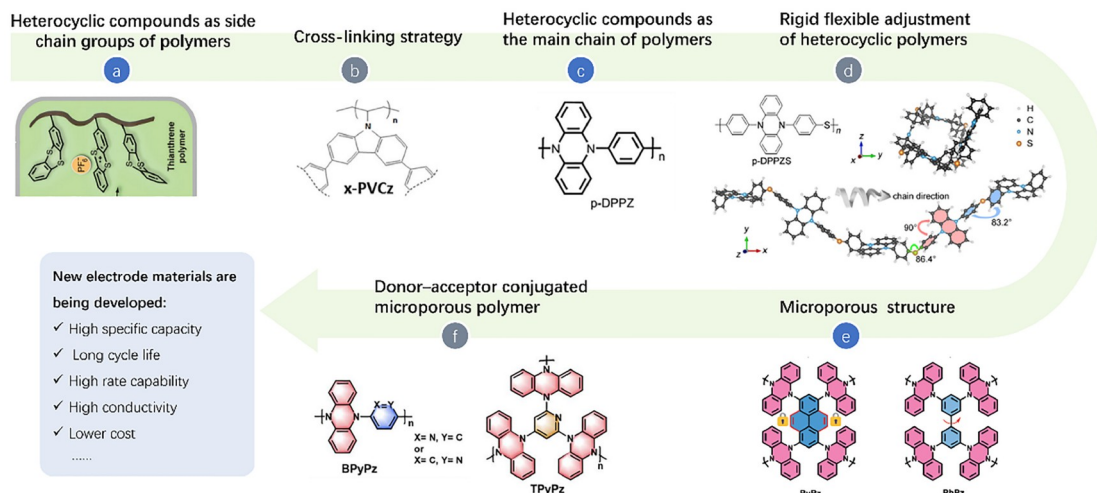


**Figure 11** Research progress in heterocyclic organic polymers. (a) Heterocyclic compounds as side chain groups in polymers. Reproduced with permission [135]. Copyright 2015, the Royal Society of Chemistry. (b) Cross-linking strategy. Reproduced with permission [156]. Copyright 2021, Elsevier. (c) Heterocyclic compounds as the main chain of polymers. Reproduced with permission [160]. Copyright 2019, Elsevier. (d) Rigid flexible adjustment of heterocyclic polymers. Reproduced with permission [165]. Copyright 2019, Elsevier. (e, f) Microporous and donor–acceptor structural design [70,71] (color online).

### 3.3 Bipolar polymers

Bipolar organic compounds may be promising candidates for utilization in metal-ion batteries and DIBs [166]. The bipolar electrode usually comprises redox-active n-type organic compounds and p-type organic compounds, which can be used as electron donors and acceptors, requiring cations and anions as charge carriers, respectively. Only one bipolar organic material can be used for both the cathode and anode to assemble symmetric batteries [167]. By contrast, bipolar compounds generally exhibit a higher capacity and a wide voltage range owing to their ability to store both anions and cations. Bipolar electrodes in symmetrical cells use a part of the capacity of bipolar compounds and their voltage ranges. For instance, a sequence of alternating n-type anthraquinone (AQ) units and p-type 5,10-dihydrophenazine (DPZ) units result in poly[anthraquinone-*alt*-dihydrophenazine] (PAQDPZ) [133]. The PAQDPZ material in the half cell exhibits a specific capacity of approximately 250 mAh g<sup>-1</sup> within the voltage range 1.6–4.3 V. However, the symmetric battery based on PAQDPZ exhibits a reversible capacity of only 105 mAh g<sup>-1</sup>. Bipolar polymers include covalent organic frameworks (COFs) with interconnected n-type and p-type organic compounds and macrocyclic molecules (mainly porphyrin and phthalocyanine) (Table 4).

#### 3.3.1 Bipolar COF

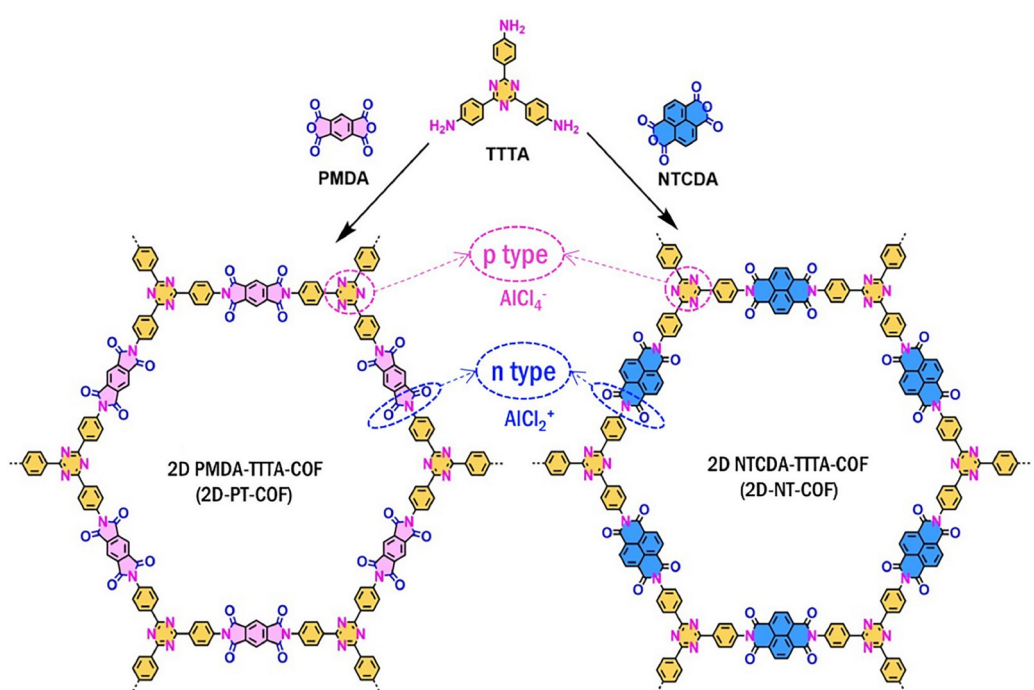
High rigidity and large polymerization degree are the inherent properties of COFs, which contribute to the enhanced stability of redox moieties, resulting in their strong resistance to dissolution, which is favorable for the development of electrode materials with extended cycling durability [172].

For instance, p-type quaternary nitrogen centers and n-type imide units make up the bipolar polyimide COF [168]. The storage of Li<sup>+</sup> and PF<sub>6</sub><sup>-</sup> can be facilitated by the redox processes of anionic imide radicals and cationic nitrogen-center radicals, respectively, and it results in a high capacity of 165 mAh g<sup>-1</sup> and a capacity retention of 91% for 4,000 cycles. Another study proposed the synthesis of two two-dimensional (2D) COFs, namely 2D-PT-COF and 2D-NT-COF (Figure 12) [169]. These materials demonstrated the redox-bipolar characteristic with the incorporation of the n-type imide and p-type triazine moieties within a single framework.

COFs include other types in addition to the PI type. A COF, which is composed of a p-type viologen block and an n-type triazine-containing triamine-phenyl-triazine block, could function in storing both anions and cations (Figure 13). This porous organic framework exhibited innovative modes of co-storage for multiple ions, specifically PF<sub>6</sub><sup>-</sup>/Li<sup>+</sup>, OTF<sup>-</sup>/Mg<sup>2+</sup>, and OTF<sup>-</sup>/Zn<sup>2+</sup> [170]. The Coulombic interactions between positively charged cationic carriers and negatively charged anionic carriers within the framework considerably affected electrode kinetics. These interactions effectively enhanced the migration of fast ion carriers toward the interior of the framework, leading to improved electrode performance. Therefore, the use of the PF<sub>6</sub><sup>-</sup>/Li<sup>+</sup> co-storage mode in the framework demonstrates a notable ED of 878 Wh kg<sup>-1</sup> for more than 20,000 cycles. Additionally, this storage exhibits a commendable PD of 28 kW kg<sup>-1</sup>, which is on par with commercially available supercapacitors. The co-storage mode, which enhances both energy and power densities, can facilitate the investigation of novel electrodes that are not typical in conventional single-ion electrodes.

**Table 4** Electrochemical performance comparison of bipolar compounds, bipolar COF, bipolar porphyrin and phthalocyanine

	Cathode	Voltage	Specific capacity	Cycling capability
Li-DIB	PAQDPZ [133]	2.85 V	246/205/187/174/134 mAh g <sup>-1</sup> @100/200/500/800/1,000/2,000 mA g <sup>-1</sup>	85% for 1,000 cycles@2 A g <sup>-1</sup>
Li-DIB	PAQDPZ [133]	1.2 V	98/90/85/81/79/78 mAh g <sup>-1</sup> @100/200/300/400/500/800 mA g <sup>-1</sup>	68% for 400 cycles@200 mA g <sup>-1</sup>
Li-DIB	NT-PICOF [168]	1.5~4.25 V	165 mAh g <sup>-1</sup> @30 mA g <sup>-1</sup>	91% for 4,000 cycles@1,000 mA g <sup>-1</sup>
Al-DIB	2D-NT-COF [169]	~1.3 V	132 mAh g <sup>-1</sup> @0.1 A g <sup>-1</sup> 79 mAh g <sup>-1</sup> @1,6 A g <sup>-1</sup>	97% for 4,000 cycles@1 A g <sup>-1</sup>
Li-DIBs	Ion co-storage framework [170]	1.5~4.5 V	348 mAh g <sup>-1</sup> @0.5 C  199 mAh g <sup>-1</sup> @0.1 A g <sup>-1</sup>	20,000 cycles@37.5 C
Li-DIB	T4PP [125]	1.0~4.5 V	113, 110, 106, 103 and 102 mAh g <sup>-1</sup> @0.1, 1, 3, 5, 7 and 9 A g <sup>-1</sup>	80% for 5,000 cycles@1 A g <sup>-1</sup>
Na-DIB	T4PP [125]	1.0~4.5 V	134, 112, 101, 91 and 76 mAh g <sup>-1</sup> @0.1, 0.3, 0.5, 0.7 and 1 A g <sup>-1</sup>	92.5% for 200 cycles@0.2 A g <sup>-1</sup>
Li-DIB	CuT4PP [125]	1.0~4.5 V	~300 mAh g <sup>-1</sup> @0.1 A g <sup>-1</sup> (1st) 139 mAh g <sup>-1</sup> @0.1 A g <sup>-1</sup> (10th)	~50% for 50 cycles@0.1 A g <sup>-1</sup>
Na-DIB	CuT4PP [125]	1.0~4.5 V	134 mAh g <sup>-1</sup> @0.2 A g <sup>-1</sup> (1st) 199 mAh g <sup>-1</sup> @0.2 A g <sup>-1</sup> (9th)	~55% for 200 cycles@0.2 A g <sup>-1</sup>
Iodine DIB	Zn-TCPP [126]	0.4 V~1.6 V 1.25 V	278 mAh g <sup>-1</sup> @5 A g <sup>-1</sup> 456, 408, 358, 308, 278 and 211 mAh g <sup>-1</sup> @1, 2, 3, 4, 5 and 10 A g <sup>-1</sup>	68% for 5,000 cycles@5 A g <sup>-1</sup>
Li-DIB	CuTAPc [127]	1.5~4.5 V	236 mAh g <sup>-1</sup> @50 mA g <sup>-1</sup> 150 mAh g <sup>-1</sup> @0.2 A g <sup>-1</sup>	49.6% for 4,000 cycles@4 A g <sup>-1</sup>
Organic symmetric DIB	TP [171]	2.7 V	136, 121, 114, 107 and 97 mAh g <sup>-1</sup> @0.2, 0.3, 0.5, 1 and 2 A g <sup>-1</sup>	62.5% for 1,500 cycles@1 A g <sup>-1</sup>

**Figure 12** The structures and synthesis routes of 2D-PT-COF and 2D-NT-COF [169] (color online).

### 3.3.2 Bipolar porphyrin and phthalocyanine

Porphyrin and phthalocyanine are typically planar and aromatic macrocyclic molecules, which exhibit bipolar char-

acteristics because of their ability to either donate or accept electrons [173]. The oxidation or reduction of these molecules results in a change in the number of  $\pi$ -electrons. Spe-

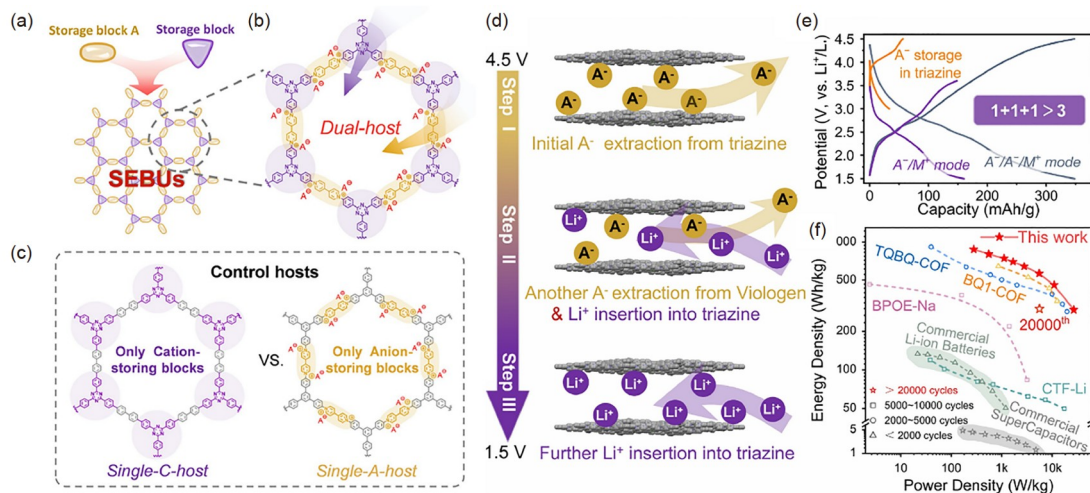


**Figure 13** The constructing route, structure, mechanism and electrochemical performance of multiple-ion and single-ion hosts. (a) Schematic illustration of constructing multiple-ion co-storage host via SEBUs strategy. (b) Chemical structure of dual-host for  $\text{A}^-/\text{M}^+$  co-storage. (c) Chemical structures of the control  $\text{M}^{n+}$ -host and  $\text{A}^-$ -host.  $\text{M}^{n+}$  denotes metal cations;  $\text{A}^-$  denotes anions. (d) Schematic illustration of  $\text{A}^-/\text{A}^-/\text{M}^+$  triple-mode discharge process. (e) Corresponding galvanostatic discharge/charge curves of  $\text{A}^-/\text{A}^-/\text{M}^+$  triple-mode,  $\text{A}^-/\text{M}^+$  mode, and high-voltage triazine p-type redox. (f) Comparison of typical energy and power densities of organic electrodes. Reproduced with permission [170]. Copyright 2023, Wiley-VCH (color online).

specifically, the 18  $\pi$ -electrons of porphyrin can be oxidized to 16  $\pi$ -electrons, whereas the 18  $\pi$ -electrons of phthalocyanine can be reduced to 20  $\pi$ -electrons [171]. Additionally, the narrow HOMO–LUMO gaps exhibited by these materials can facilitate the efficient transfer of electrons, leading to rapid redox kinetics. Furthermore, the presence of highly stable C–N bonds within their frameworks confers a substantial reversible capacity and working voltage. Studies have documented the use of porphyrin/phthalocyanine-based derivatives or polymers as electrode materials for electrochemical EESs within this framework.

The stability of porphyrin compounds is higher than that of other organic electrode materials, primarily attributable to their rigid and extended frameworks (Table 4). The team led by Chen and Gao [125] proposed a novel proposition involving the use of a metal-free porphyrin complex, specifically 5,10,15,20-tetra(4-pyridinyl)-21H,23H-porphyrin (T4PP), and its copper-containing counterpart (CuT4PP), as potential electrode materials. This molecule exhibited a mixed charge-storage mechanism involving both p-type and n-type characteristics. The distinctive attributes of T4PP and CuT4PP resulted in several versatile functionalities, rendering them suitable for various applications, such as in Li-DIBs and Na-DIBs. It is worth noting that CuT4PP shows a higher specific capacity at low current density than T4PP; however, the cycling stability of CuT4PP is worse than that of T4PP. The incorporation of pyridine groups into the extended porphyrin conjugated structure resulted in a long cycle life of 5,000 cycles and a high PD of  $18.7 \text{ kW kg}^{-1}$ . Moreover, the incorporation of both cations and anions in a hybrid charge-storage mechanism facilitated rapid charge transfer, resulting in enhanced performance.

The use of 2D coordinated supramolecular networks (2D CSNs) enables a highly effective process of anchoring and conversion of anions, which can be attributed to the substantial specific surface area, high electrical conductivity, and abundant active sites. A study investigated a 2D porphyrin-CSN cathode (Zn-TCPP), for its potential application in aqueous iodine DIBs [126]. The Zn-TCPP cathode exhibited a remarkable specific capacity of  $278 \text{ mAh g}^{-1}$ , corresponding to an ED of  $340 \text{ Wh kg}^{-1}$ . Additionally, the cathode demonstrated a high ED at a current density of  $5 \text{ A g}^{-1}$  with a durable cycle performance of 5,000 cycles and a high CE of 98%. The 2D layered network structure of Zn-TCPP could efficiently facilitate the penetration of  $\text{I}_3^-$  (Figure 14). This study investigated the binding of  $\text{I}_3^-$  ions with 2D porphyrin-CSN by using molecular orbital theory and the 2D layered network structural analysis. These findings formed a basis for the wider application of 2D CSNs in energy storage and the advancement of iodine-based DIBs cathodes.

The multifunctionality of the self-polymerizable bipolar Cu tetraaminephthalocyanine (CuTAPc) [127] could be used in various EESs (Figure 15). The use of CuTAPc as the cathode material in Li-DIBs led to a substantial discharge capacity of  $236 \text{ mAh g}^{-1}$  at a current density of  $50 \text{ mA g}^{-1}$ . Furthermore, CuTAPc exhibited an impressive reversible capacity of  $74.3 \text{ mAh g}^{-1}$  even after 4,000 cycles at a current density of  $4 \text{ A g}^{-1}$ . Interestingly, all-organic symmetric DIBs could achieve a high ED of  $239 \text{ Wh kg}^{-1}$  and PD of  $11.5 \text{ kW kg}^{-1}$ .

In conclusion, combining the electrochemical properties of the bipolar compounds, bipolar COF and bipolar porphyrin and phthalocyanine, we can conclude that the bipolar com-

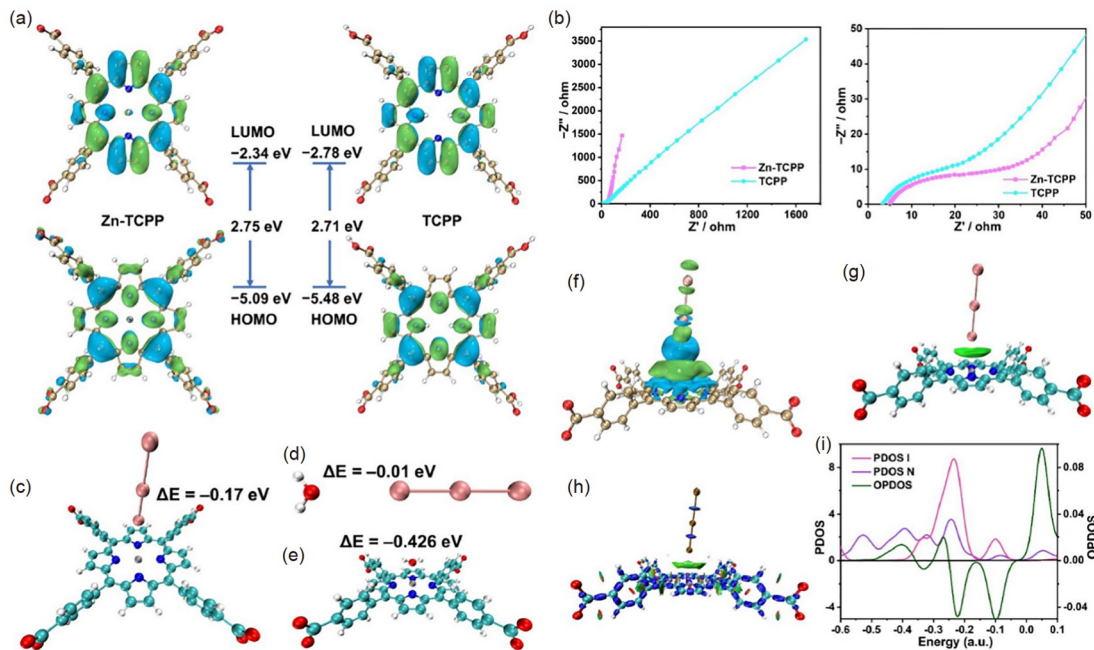


**Figure 14** (a) HOMOs and LUMOs, (b) electrical impedance spectroscopy curves of the Zn-TCPP and TCPP cathode. (c,d) Adsorption configuration and adsorption energies of  $\text{I}_3^-$  on (c) Zn-TCPP, and (d)  $\text{H}_2\text{O}$ . (e) Adsorption configuration and adsorption energy of  $\text{H}_2\text{O}$  on Zn-TCPP. (f) Isosurface map of EDD of Zn-TCPP/ $\text{I}_3^-$ . Green isosurfaces are for the increase of electron density, while the blue are for the decrease. Isosurface value is set as 0.0001. (g) Isosurface map of IGMH of Zn-TCPP/ $\text{I}_3^-$ . (h) Isosurface map of IRI of Zn-TCPP/ $\text{I}_3^-$ . Green isosurfaces are attributed to weak interactions while the blue are assigned to chemical bonds. (i) PDOS and OPDOS of Zn-TCPP/ $\text{I}_3^-$ . Reproduced with permission [126]. Copyright 2023, Wiley-VCH (color online).

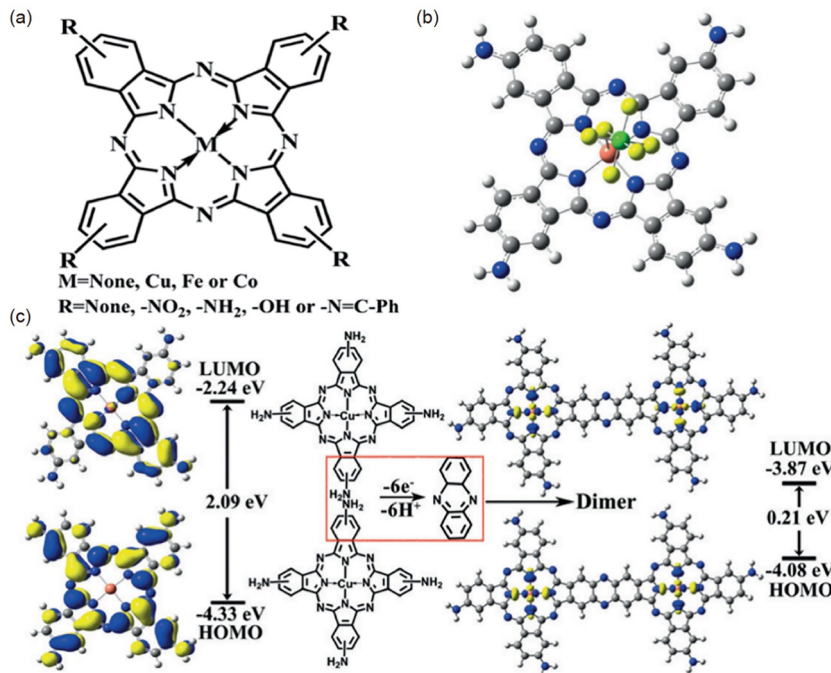


**Figure 15** The structure, geometry and DFT calculations of the phthalocyanine derivatives. (a) Molecular structure of the various phthalocyanine derivatives. (b) Geometry of  $\text{PF}_6^-$ -binding to CuTAPc. (c) Energy level diagrams of CuTAPc and its dimer obtained from DFT calculations. Reproduced with permission [127]. Copyright 2019, Wiley-VCH (color online).

pounds show high specific capacities, and some of them are even close to  $300 \text{ mA g}^{-1}$ . However, the discharge plateau

voltage of bipolar cathodes is low, which results in the full battery device with a relatively low energy density.

### 3.4 All-carbon-unsaturated compounds

All-carbon-unsaturated compounds are a class of hydrocarbons comprising only carbon and hydrogen. These compounds contain carbon–carbon double bonds, carbon–carbon triple bonds, or aromatic rings. Some all-carbon-unsaturated compounds reported in the literature include poly(*para*-phenylene) (PPP), pyrene, polypyrenes, and graphdiyne (GDY).

Poly(*para*-phenylene) (PPP) exhibits high electrical conductivity when doped with either electron donors (n-doping) or electron acceptors (p-doping). The PPP cathode undergoes p-type reactions during the charging process in which it loses an electron and reacts with anions. Thus, due to notable characteristics such as elevated voltages (approximately 3.95 V) and exceptional cycling stability (770 cycles) even under high current density conditions of  $1,000 \text{ mA g}^{-1}$ , the PPP cathode can be a reliable cathode material in K-DIBs [137]. Moreover, when a K-DIB full cell was used, with a graphite anode paired with a PPP cathode, it exhibited an ED of  $106 \text{ Wh kg}^{-1}$ , remarkable rate performance, and the ability to undergo 500 cycles at a high current density of  $1,000 \text{ mA g}^{-1}$ , demonstrating excellent long-term cycling performance.

Pyrene ( $C_{th}$  is  $133 \text{ mAh g}^{-1}$ ), obtained through the distillation of coal tar, is an inexpensive material. It can reversibly store anions during redox reactions by stabilizing the positive charge by four aromatic rings [174]. However, crystalline monomeric pyrene exhibits non-significant charge–storage capacities, and the use of amorphous polypyrene yielded excellent electrochemical performance. Thus, a combination of polypyrenes exhibiting diverse linking patterns and electronic structures can be used as OEs capable of hosting  $\text{Cl}^-$  ions in aqueous Zn-DIBs [72]. Comparative investigation revealed that the polypyrenes’ redox activity can be controlled by changing the connecting patterns on the pyrene unit, and the electronic structures are crucial. The polymer cross-linked pyrene with interconnected structures exhibited a higher capacity than the linear counterparts. The difference can be attributed to the high surface area and a narrow band gap.

GDY [136] is the cathode material for Al-DIBs, hosting the diffusing  $\text{AlCl}_4^-$  responsible for charging/discharging. DFT calculations and thermodynamic stability assessment were used to investigate  $\text{AlCl}_4^-$  adsorption on the GDY. The results showed that  $C_{th}$  of this system at ambient temperature was  $186 \text{ mAh g}^{-1}$ , which is three times as high as that when using graphite as the cathode.

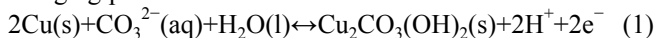
In summary, four types of anion-hosting organic cathodes, including aromatic amine polymers, heterocyclic polymers, bipolar compounds, and all-carbon-unsaturated compounds, are described in detail. In general, organic electrode materials have higher theoretical capacities than traditional gra-

phite cathodes. Secondly, their anion reaction potentials are low compared with the intercalation potentials of graphite, reducing side reactions with electrolytes in high potentials, and thus giving good cycling stabilities. More importantly, the structural design of organic materials and the regulation of polymer segments can realize the adjustment of theoretical capacity, conductivity, and cycle stability, which are crucial for the performance of DIBs.

## 4 Conversion-type cathodes

Unlike graphite and organic cathodes, the use of a metal as a cathode involves the conversion of the metal into its corresponding metal salt, enabling every atom of the metal to accommodate anions through the formation of ionic bonds. Consequently, this mechanism leads to an increase in specific capacity. Until 2011, metals could reversibly store  $\text{F}^-$ , defined as the fluoride ion battery (FIB), as reported in the literature [175]. The reaction mechanism of FIBs can be described as follows: during the discharge process, electrons are produced at the anode by a thermodynamically favorable and spontaneous redox reaction. Electrons traverse an external circuit to undergo recombination with the cathode material, resulting in the reduction of the metal fluoride to metal M. The released  $\text{F}^-$  moves away from the cathode, traverses through the electrolyte, and undergoes a reaction with the metal M' present at the anode, resulting in the formation of metal fluoride  $\text{M}'\text{F}_x$ , thereby maintaining electro-neutrality. Batteries with  $\text{CuF}_2$ ,  $\text{BiF}_3$  (both composite and solid solution),  $\text{SnF}_2$ , and  $\text{KBiF}_4$  as the cathode and Ce metal as the anode were tested at  $150^\circ\text{C}$ , which revealed the specific capacities of  $322 \text{ mAh g}^{-1}$  ( $C_{th} = 527 \text{ mAh g}^{-1}$ ),  $126/190 \text{ mAh g}^{-1}$  ( $C_{th} = 302 \text{ mAh g}^{-1}$ ),  $177 \text{ mAh g}^{-1}$  ( $C_{th} = 230 \text{ mAh g}^{-1}$ ), and  $183 \text{ mAh g}^{-1}$  ( $C_{th} = 342 \text{ mAh g}^{-1}$ ), respectively. Similarly, the use of metal halides as electrode materials, in which  $\text{Cl}^-$  are charge carriers, has attracted considerable attention [176,177].

Investigation of copper as the cathode in an  $8.5 \text{ mol L}^{-1}$  KOH electrolyte showed that the copper cathode exhibits a high initial capacity of  $300 \text{ mAh g}^{-1}$  through reversibly storing  $\text{OH}^-$ . However, the efficacy of the copper electrode decayed rapidly within the alkaline electrolyte [178]. Ji et al. [73] reported that the Cu electrode can reversibly store  $\text{CO}_3^{2-}$  and  $\text{OH}^-$  anions. In its initial cycle, the Cu electrode exhibited a reversible capacity of  $412 \text{ mAh g}^{-1}$  at a current rate of  $0.5 \text{ A g}^{-1}$  (Figure 16a). The *ex-situ* XRD results showed that the malachite phase  $\text{Cu}_2\text{CO}_3(\text{OH})_2$  was a result of anodic charging, with both  $\text{CO}_3^{2-}$  and  $\text{OH}^-$  anions acting as charge-compensating carriers. The description of a two-phase conversion in Equation 1 is supported by the single-plateau charging profile.



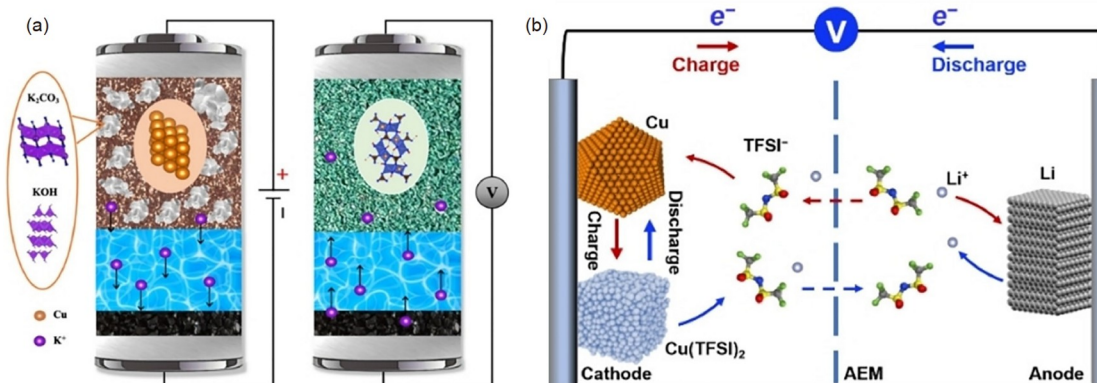


**Figure 16** (a) Cu as the cathode to reversibly store  $\text{CO}_3^{2-}$  and  $\text{OH}^-$  anions in aqueous electrolytes and (b) Cu as the cathode to reversibly store  $\text{TFSI}^-$  anions in organic electrolytes. Reproduced with permission [73,74]. Copyright 2022, Wiley-VCH (color online).

To explore the effectiveness of copper electrodes for reversibly storing anions in organic electrolytes, the same research group revealed that bulk copper powder has highly stable cycle performance in organic electrolytes and a high reversible capacity of  $762 \text{ mAh g}^{-1}$  at  $3.2 \text{ V}$  compared with  $\text{Li}^+/\text{Li}$  (Figure 16b) [74]. Anion charge carriers are transferred when the copper electrode is in operation. The researchers created an imbalanced electrolyte using a catholyte that is less concentrated than the anolyte, which resulted in a high specific capacity and superior reversibility while addressing the problem of concentrate ion overpotential that resulted during charging. This discovery provides a positive course for high-energy DIB.

Although Cu has a high anion storage capacity in both aqueous and non-aqueous solutions, it has a poor reversible capacity. The fact that it has such terrible cycling performance is even more astonishing. For example, the capacities of Cu for 10 cycles in non-aqueous solvents and 50 cycles in non-aqueous solvents are only  $140$  and  $275 \text{ mAh g}^{-1}$ , respectively. Cycling performance can be improved to some extent if the metal is treated to make a composite material. For instance, in a dual-ion-type micro-redox capacitor (MRC), a hybrid cathode of silver nanowires (AgNWs) between MXene with bacterial cellulose as interlayers (MXene/AgNWs&BC) is synthesized for reversible storage of  $\text{Cl}^-$  [177]. It has been observed that AgNWs between MXene nanosheets can not only minimize MXene nanosheet restacking and extend the interlayer space, but also give 50% more capacity due to the extra phase transition behavior ( $\text{Ag} \leftrightarrow \text{AgCl}$ ). As a result, the resulting MRC has a greatly increased areal energy density of up to  $227 \mu\text{Wh cm}^{-2}$ , as well as significantly improved output stability and suppressed renowned self-discharge behavior. *In-situ* XRD/Raman investigations establish and disclose the reversible solid-to-solid conversion of an  $\text{Ag}/\text{AgCl}$  redox pair confined between MXene interlayers. Though  $\text{AgCl}$  has poor conductivity, which leads to poor redox reversibility of the

$\text{Ag}/\text{AgCl}$  redox couple, in the case of MXene/AgNWs&BC, the use of MXene with metallic conductivity, serving as electrons feeding bridge embracing the formed  $\text{AgCl}$ , significantly aids the slow reduction kinetics of  $\text{AgCl}$  into  $\text{Ag}$ . As a result, the redox reaction is highly reversible, which improves cycling stability. The proposed MRC realizes a large 75% capacity retention with a high Coulombic efficiency approaching 100% at a current density of  $5 \text{ mA cm}^{-2}$  over 1,000 cycles.

In conclusion, conversion-type cathodes have a high theoretical capacity and can also have a high reversible capacity, but their cycling performance is poor. As a result, enhancing the conductivity of anionic binding products and suppressing their dissolution shuttle action by structural design will be the future development direction of such compounds. Designing selective permeable membranes to inhibit the shuttle effect of dissolved anionic binding products, on the other hand, can greatly improve the electrochemical performance of conversion-type cathodes.

In addition to the anion-hosting cathodes, other anion-storage materials have been reported. For instance,  $\text{P}_3\text{Na}_{0.5}\text{Ni}_{0.25}\text{Mn}_{0.75}\text{O}_2$  was reported to store  $\text{ClO}_4^-$  anions through  $\text{O}^{2-} \rightarrow \text{O}^-$  conversion by increasing the charge cutoff voltage [179]. The  $\text{Cu}_2\text{O}$  cathode [180] could reversibly store  $\text{Cl}^-$ . A high-potential triphenylphosphine selenide organic cathode (TP-Se) was reported as the cathode of DIBs [181], and  $(\text{TP-Se})^-$  to  $(\text{TP-Se})^0$  to  $(\text{TP-Se})^+$  conversion could be used to store anions. MOF [182], and MXenes [183] were reported as dual-ion hosts.

## 5 Summary and outlook

This review summarizes the research progress and recent studies in anion-hosting cathodes for DIBs. Despite significant achievements, the current electrochemical performance of cathodes for DIBs remains insufficient for practical

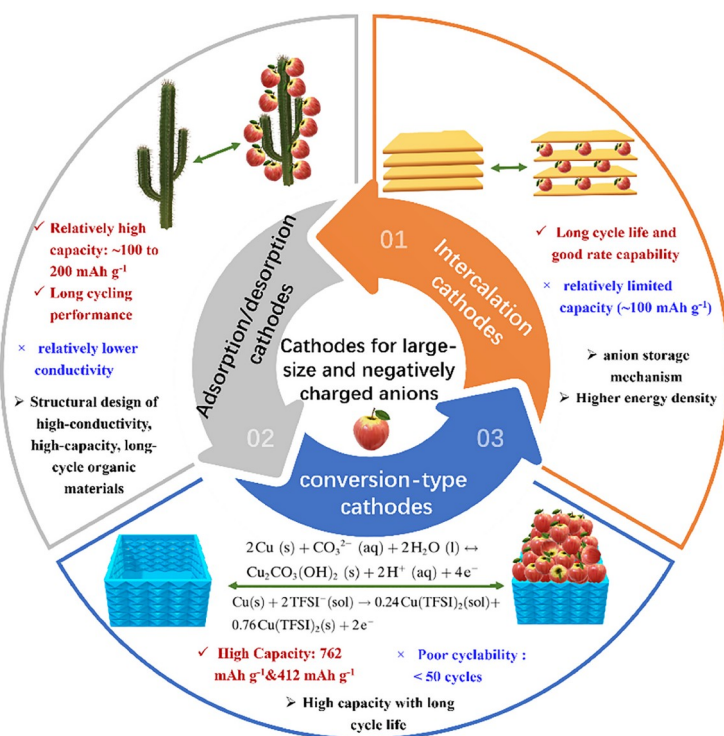


**Figure 17** Schematics of current research advances and future development direction for DIBs (color online).

utilization (Figure 17).

Graphite is a representative material that utilizes the intercalated anion storing mechanism. Its cycle stability and rate performance are reasonably high, but its theoretical capacity is poor due to the reaction properties of its intercalation. As a result, the solutions presented in this study to achieve superior graphite cathodes are based on concepts such as small-sized or light-weight charge carriers for higher ED, wasted carbon resources for lower cost, structural design and surface modification for longer cycle life, and high ED DIBs. Further studies on graphite cathodes should focus on the following aspects. (1) In-depth characterization and understanding of mechanism: develop *in-situ* characterization technologies of graphite, monitor the process of anion intercalation-de-intercalation, and integrate theoretical calculations to thoroughly investigate its capacity degradation mechanism. (2) Design and regulation of graphite: structural characteristics of graphite such as graphitization degree, interlayer space and crystallinity affect the intercalation voltage, capacity, and rate performance of the graphite cathode-based DIB. Therefore, the design and regulation of graphite structure is of great significance for the study of graphite cathode. (3) Surface engineering of graphite: the CE, cycling performance and all-climate temperature operation properties of graphite-based DIBs are affected by the morphology and composition of graphite surface, so it is of great significance to modify graphite surface by appropriate methods. (4) Consideration of the practical application: the usage of

high areal density graphite cathode in DIBs will increase the actual energy density. However, the high areal density graphite cathodes confront with huge volume expansion during the anion intercalation, which may destroy the stability of the electrode structure and lead to a decrease in cycling stability. Therefore, it is necessary to improve the cycling stability of high areal density graphite cathode in the practical application of DIBs.

Organic cathodes store anions because organic materials have reaction sites that can anchor anions (with the purpose of adsorption-desorption anions). The various organic cathode materials presented in this review are based on distinct anchor locations for doping and de-doping anions. The *C<sub>th</sub>s* of the organic materials to store anions are adjusted by the number of anchor points in the polymer chain segment. At present, the *C<sub>th</sub>s* of most organic electrode materials are higher than the theoretical capacity of graphite, and some even exceed 200 mAh g<sup>-1</sup>. Its practical specific capacity is also between 100–200 mAh g<sup>-1</sup>, which is higher than that of graphite. However, due to the twisted nature of the molecular chains, the anion may not reach the anchor position, resulting in the unusability of the anchor position, which in turn leads to the practical capacity being lower than the theoretical capacity. As a result, while designing organic cathodes based on theoretical capacity, the structural properties of the molecule should be taken into account to guarantee that theoretical capacity may be exerted to a higher degree. Second, organic material conductivity is a major

issue, and it is critical to overcome the conductivity problem of organic materials by molecular design. Third, the performance of other DIB attributes such as platform voltage, rate performance, cycle stability, ED and PD must be thoroughly considered.

Conversion-type materials store anions by changing the valence state of the metal material, and because each metal atom may store one or more anions, conversion materials have a higher  $C_{th}$  than the graphite and organic cathodes. However, metal atom oxidation results in a molecule with the solubility, or a product structure that is more stable and not easily reduced, both of which contribute to poor cycle stability of conversion materials. Therefore, possible solutions should be devised to enhance their cycle stability, such as constructing a microcapsule-structured material that limits the anion storage response to tiny units or employing superior selective permeability membranes.

To improve the performance of cathodes, optimizing the structure and the electrolyte interface of graphite-based materials is essential. In addition to the development of anion-intercalated cathode materials, other types of cathode materials (*e.g.*, coordination and conversion types) should be developed. The discovery of new anion-hosting cathode materials may open up new opportunities for the development of DIBs.

**Acknowledgements** The authors gratefully acknowledge the financial support from National Key R&D Program of China (2022YFB2402600), National Natural Science Foundation of China (52125105, 51972329), NSFC/RGC Joint Research Scheme (Project No: N\_CityU104/20 and 52061160484), Science and Technology Planning Project of Guangdong Province (2021TQ05L894), and Shenzhen Science and Technology Planning Project (JSGG20211108092801002, JSGG20220831104004008), Quality and Reform Project of Guangdong province undergraduate teaching (XQSYS-2222873), and Key Scientific Research Projects of General Universities in Guangdong Province (2021KCXTD086).

**Conflict of interest** The authors declare no conflict of interest.

- 1 Winter M, Barnett B, Xu K. *Chem Rev*, 2018, 118: 11433–11456
- 2 Zhang H, Li C, Piszcz M, Coya E, Rojo T, Rodriguez-Martinez LM, Armand M, Zhou Z. *Chem Soc Rev*, 2017, 46: 797–815
- 3 Dou Q, Wu N, Yuan H, Shin KH, Tang Y, Mitlin D, Park HS. *Chem Soc Rev*, 2021, 50: 6734–6789
- 4 Forsyth M, Porcarelli L, Wang X, Goujon N, Mecerreyres D. *Acc Chem Res*, 2019, 52: 686–694
- 5 Wang G, Yu M, Feng X. *Chem Soc Rev*, 2021, 50: 2388–2443
- 6 Wang B, Xie PY, Zhang M, Zhang HT, Chen YS. *Sci China Technol Sci*, 2022, 65: 2866–2873
- 7 Ou X, Gong D, Han C, Liu Z, Tang Y. *Adv Energy Mater*, 2021, 11: 2102498
- 8 Xue S, Shang J, Pu X, Cheng H, Zhang L, Wang C, Lee CS, Tang Y. *Energy Storage Mater*, 2023, 55: 33–41
- 9 Zhao X, Zhao-Karger Z, Fichtner M, Shen X. *Angew Chem Int Ed*, 2020, 59: 5902–5949
- 10 Xie D, Zhang M, Liu Q, Lin Y, Yu A, Tang Y. *Adv Funct Mater*, 2023, 33: 2306291
- 11 Chen C, Lee CS, Tang Y. *Nano-Micro Lett*, 2023, 15: 121
- 12 Cai P, Sun W, Chen J, Chen K, Lu Z, Wen Z. *Adv Energy Mater*, 2023, 13: 2301279
- 13 Yuan J, Yu B, Pan D, Hu X, Chen J, Aminua M, Liu Y, Sheng LM, Chen Y, Wu Y, Zhan H, Wen Z. *Adv Funct Mater*, 2023, 33: 2305503
- 14 Zhang M, Li H, Chen J, Ma FX, Zhen L, Wen Z, Xu CY. *Adv Funct Mater*, 2023, 33: 2303189
- 15 Holoubek J, Chen Z, Liu P. *ChemSusChem*, 2023, 16: e202201245
- 16 He Y, Dong Y, Zhang Y, Li Y, Li H. *Adv Sci*, 2023, 10: 2207426
- 17 Das S, Manna SS, Pathak B. *ChemSusChem*, 2023, 16: e202201405
- 18 Zhang X, Tang Y, Zhang F, Lee CS. *Adv Energy Mater*, 2016, 6: 1502588
- 19 Xu J, Ma J, Fan Q, Guo S, Dou S. *Adv Mater*, 2017, 29: 1606454
- 20 Placke T, Heckmann A, Schmuck R, Meister P, Beltrup K, Winter M. *Joule*, 2018, 2: 2528–2550
- 21 Tebyetekerwa M, Duignan TT, Xu Z, Song Zhao X. *Adv Energy Mater*, 2022, 12: 2202450
- 22 Yu D, Li K, Ma G, Ru F, Zhang X, Luo W, Hu P, Chen D, Wang H. *ChemSusChem*, 2023, 16: e202201595
- 23 Zheng T, Xiong J, Zhu B, Shi X, Cheng YJ, Zhao H, Xia Y. *J Mater Chem A*, 2021, 9: 9307–9318
- 24 Jin J, Liu Y, Pang X, Wang Y, Xing X, Chen J. *Sci China Chem*, 2021, 64: 385–402
- 25 Gong D, Wei C, Liang Z, Tang Y. *Small Sci*, 2021, 1: 2100014
- 26 Rajagopalan R, Tang Y, Ji X, Jia C, Wang H. *Adv Funct Mater*, 2020, 30: 1909486
- 27 Zhang W, Yin J, Wang W, Bayhan Z, Alshareef HN. *Nano Energy*, 2021, 83: 105792
- 28 Sun L, Li G, Zhang S, Liu S, Yuwono J, Mao J, Guo Z. *Sci China Chem*, 2024, 67: 4–12
- 29 Wang M, Liu Q, Wu G, Ma J, Tang Y. *Green Energy Environ*, 2023, 8: 548–558
- 30 Tong Z, Kang T, Wu Y, Zhang F, Tang Y, Lee CS. *Nano Res*, 2022, 15: 7220–7226
- 31 Lei X, Liang X, Yang R, Zhang F, Wang C, Lee CS, Tang Y. *Small*, 2022, 18: 2200418
- 32 Wang G, Wang Z, Shi H, Du A, Sun M, Cui G. *Sci China Chem*, 2024, 67: 214–246
- 33 Shi Y, Chen Y, Shi L, Wang K, Wang B, Li L, Ma Y, Li Y, Sun Z, Ali W, Ding S. *Small*, 2020, 16: 2000730
- 34 Zheng L, Yang H, Bai Y, Wu C. *J Energy Chem*, 2021, 60: 229–232
- 35 Chen Z, Ren W, Gao L, Liu B, Pei S, Cheng HM. *Nat Mater*, 2011, 10: 424–428
- 36 Lin MC, Gong M, Lu B, Wu Y, Wang DY, Guan M, Angell M, Chen C, Yang J, Hwang BJ, Dai H. *Nature*, 2015, 520: 324–328
- 37 Elia GA, Marquardt K, Hoepfner K, Fantini S, Lin R, Knipping E, Peters W, Drillet J-, Passerini S, Hahn R. *Adv Mater*, 2016, 28: 7564–7579
- 38 Ji B, He H, Yao W, Tang Y. *Adv Mater*, 2021, 33: 2005501
- 39 Wang M, Jiang C, Zhang S, Song X, Tang Y, Cheng HM. *Nat Chem*, 2018, 10: 667–672
- 40 Zeng F, Li S, Hu S, Qiu M, Zhang G, Li M, Chang C, Wang H, Xu M, Zheng L, Tang Y, Han C, Cheng HM. *Adv Funct Mater*, 2023, 33: 2302397
- 41 Xu X, Yang H, Wang X, Wang D, Hu X, Peng C. *Cell Rep Phys Sci*, 2022, 3: 100981
- 42 Zhang L, Wang H, Zhang X, Tang Y. *Adv Funct Mater*, 2021, 31: 2010958
- 43 Zhou W, Zhang M, Kong X, Huang W, Zhang Q. *Adv Sci*, 2021, 8: 2004490
- 44 Liu M, Zhang W, Zheng W. *ChemSusChem*, 2023, 16: e202201375
- 45 Li J, Hui KS, Dinh DA, Wu S, Fan X, Chen F, Hui KN. *Mater Today Sustainability*, 2022, 19: 100188
- 46 Wu N, Zhou X, Kidkhunthod P, Yao W, Song T, Tang Y. *Adv Mater*, 2021, 33: 2101788
- 47 Jiang B, Kong T, Cai Z, Zhu W, Xiao R. *Electrochim Acta*, 2022, 435: 141402
- 48 Wang H, Wang C, Zhang F, Zhang X, Lee CS, Tang Y. *Chem Eng J*,

- 2022, 449: 137708
- 49 Tan L, Sun Y, Wei C, Tao Y, Tian Y, An Y, Zhang Y, Xiong S, Feng J. *Small*, 2021, 17: 2007717
- 50 Peng M, Shin K, Jiang L, Jin Y, Zeng K, Zhou X, Tang Y. *Angew Chem Int Ed*, 2022, 61: e202206770
- 51 Hao R, Lan H, Kuang C, Wang H, Guo L. *Carbon*, 2018, 128: 224–230
- 52 Dewar D, Glushenkov AM. *Energy Environ Sci*, 2021, 14: 1380–1401
- 53 Liu W, Liu P, Mitlin D. *Adv Energy Mater*, 2020, 10: 2002297
- 54 Qian K, Li L, Yang D, Wang B, Wang H, Yuan G, Bai J, Ma S, Wang G. *Adv Funct Mater*, 2023, 33: 2213009
- 55 Zhang X, Zhu H, He Q, Xiong T, Wang X, Xiao Z, Wang H, Zhao Y, Xu L, Mai L. *Adv Funct Mater*, 2022, 32: 2205330
- 56 Pan Q, Tong Z, Su Y, Zheng Y, Shang L, Tang Y. *Adv Mater*, 2022, 34: 2203485
- 57 Wang S, Guan Y, Gan F, Shao Z. *ChemSusChem*, 2023, 16: e202201373
- 58 Wang Y, Wang H. *ACS Appl Energy Mater*, 2022, 5: 2366–2374
- 59 Wang B, Huang Y, Wang Y, Wang H. *Adv Funct Mater*, 2023, 33: 2212287
- 60 Wang Y, Wang H. *J Energy Chem*, 2022, 75: 378–382
- 61 Zhang H, Guo G, Adenius H, Qin B, Li H, Passerini S, Huang W. *Mater Today*, 2022, 53: 162–172
- 62 Yu D, Zhu Q, Cheng L, Dong S, Zhang X, Wang H, Yang N. *ACS Energy Lett*, 2021, 6: 949–958
- 63 Zhang M, Song X, Ou X, Tang Y. *Energy Storage Mater*, 2019, 16: 65–84
- 64 Ji B, Zhang F, Wu N, Tang Y. *Adv Energy Mater*, 2017, 7: 1700920
- 65 Wu J, Wang X, Liu Q, Wang S, Zhou D, Kang F, Shammukaraj D, Armand M, Rojo T, Li B, Wang G. *Nat Commun*, 2021, 12: 5746
- 66 Wang B, Wang Y, Huang Y, Zhang L, Ma S, Wang H. *ACS Appl Energy Mater*, 2021, 4: 5316–5325
- 67 Zhang K, Li D, Shao J, Jiang Y, Lv L, Shi Q, Qu Q, Zheng H. *Small*, 2023, 19: 2206360
- 68 Zhang M, Pei Y, Liu W, Liang R, Deng YP, Chen Z, Yu A. *Nano Energy*, 2021, 81: 105643
- 69 Yang K, Liu Q, Zheng Y, Yin H, Zhang S, Tang Y. *Angew Chem Int Ed*, 2021, 60: 6326–6332
- 70 Ma W, Luo LW, Huang X, Dong P, Chen Y, Zhang C, Huang F, Jiang JX, Cao Y. *Adv Energy Mater*, 2023, 13: 2203253
- 71 Ma W, Luo LW, Dong P, Zheng P, Huang X, Zhang C, Jiang JX, Cao Y. *Adv Funct Mater*, 2021, 31: 2105027
- 72 Zhang C, Ma W, Han C, Luo LW, Daniyar A, Xiang S, Wu X, Ji X, Jiang JX. *Energy Environ Sci*, 2021, 14: 462–472
- 73 Gallagher TC, Wu CY, Lucero M, Sandstrom SK, Hagglund L, Jiang H, Stickle W, Feng Z, Ji X. *Angew Chem Int Ed*, 2022, 61: e202203837
- 74 Yu M, Sui Y, Sandstrom SK, Wu CY, Yang H, Stickle W, Luo W, Ji X. *Angew Chem Int Ed*, 2022, 61: e202212191
- 75 Luo P, Zheng C, He J, Tu X, Sun W, Pan H, Zhou Y, Rui X, Zhang B, Huang K. *Adv Funct Mater*, 2022, 32: 2107277
- 76 Rüdorff W, Hofmann U. *Z Anorg Allg Chem*, 1938, 238: 1–50
- 77 McCullough CP, Levine CA, Snelgrove RV. US patents 4380938, 1989
- 78 Carlin RT, De Long HC, Fuller J, Trulove PC. *J Electrochem Soc*, 1994, 141: L73–L76
- 79 Seel JA, Dahn JR. *J Electrochem Soc*, 2000, 147: 892–898
- 80 Wang H, Yoshio M. *Chem Commun*, 2010, 46: 1544–1546
- 81 Gualberto GM, Underhill C, Leung SY, Dresselhaus G. *Phys Rev B*, 1980, 21: 862–868
- 82 Elia GA, Hasa I, Greco G, Diemant T, Marquardt K, Hoeppner K, Behm RJ, Hoell A, Passerini S, Hahn R. *J Mater Chem A*, 2017, 5: 9682–9690
- 83 Zheng Y, Deng T, Yue N, Zhang W, Zhu X, Yang H, Chu X, Zheng W. *J Raman Spectr*, 2021, 52: 2119–2130
- 84 Huang Q, Wang L, Xu Z, Wang W, Bai X. *Sci China Chem*, 2018, 61: 222–227
- 85 Greco G, Elia GA, Hermida-Merino D, Hahn R, Raoux S. *Small Methods*, 2023, 7: 2201633
- 86 Angell M, Pan CJ, Rong Y, Yuan C, Lin MC, Hwang BJ, Dai H. *Proc Natl Acad Sci USA*, 2017, 114: 834–839
- 87 Kim KI, Guo Q, Tang L, Zhu L, Pan C, Chang CH, Razink J, Lerner MM, Fang C, Ji X. *Angew Chem Int Ed*, 2020, 59: 19924–19928
- 88 Kim KI, Tang L, Mirabedini P, Yokoi A, Muratli JM, Guo Q, Lerner MM, Gotoh K, Greaney PA, Fang C, Ji X. *Adv Funct Mater*, 2022, 32: 2112709
- 89 Yang C, Chen J, Ji X, Pollard TP, Lü X, Sun CJ, Hou S, Liu Q, Liu C, Qing T, Wang Y, Borodin O, Ren Y, Xu K, Wang C. *Nature*, 2019, 569: 245–250
- 90 Guo Q, Kim KI, Li S, Scida AM, Yu P, Sandstrom SK, Zhang L, Sun S, Jiang H, Ni Q, Yu D, Lerner MM, Xia H, Ji X. *ACS Energy Lett*, 2021, 6: 459–467
- 91 Cai S, Chu X, Liu C, Lai H, Chen H, Jiang Y, Guo F, Xu Z, Wang C, Gao C. *Adv Mater*, 2021, 33: 2007470
- 92 Meng J, Zhu L, Haruna AB, Ozoemena KI, Pang Q. *Sci China Chem*, 2021, 64: 1888–1907
- 93 Wu Y, Gong M, Lin MC, Yuan C, Angell M, Huang L, Wang DY, Zhang X, Yang J, Hwang BJ, Dai H. *Adv Mater*, 2016, 28: 9218–9222
- 94 Chen H, Guo F, Liu Y, Huang T, Zheng B, Ananth N, Xu Z, Gao W, Gao C. *Adv Mater*, 2017, 29: 1605958
- 95 Wang DY, Wei CY, Lin MC, Pan CJ, Chou HL, Chen HA, Gong M, Wu Y, Yuan C, Angell M, Hsieh YJ, Chen YH, Wen CY, Chen CW, Hwang BJ, Chen CC, Dai H. *Nat Commun*, 2017, 8: 14283
- 96 Wang S, Jiao S, Tian D, Chen HS, Jiao H, Tu J, Liu Y, Fang DN. *Adv Mater*, 2017, 29: 1606349
- 97 Wang S, Kravchyk KV, Krumeich F, Kovalenko MV. *ACS Appl Mater Interfaces*, 2017, 9: 28478–28485
- 98 Han C, Wang H, Wang Z, Ou X, Tang Y. *Adv Mater*, 2023, 35: 2300917
- 99 Ishihara T, Yokoyama Y, Kozono F, Hayashi H. *J Power Sources*, 2011, 196: 6956–6959
- 100 Wang J, Tu J, Chang C, Zhu H. *J Power Sources*, 2021, 492: 229674
- 101 Ghosh S, Mp N, Muduli S, Bhowmik S, Martha SK. *Electrochim Acta*, 2023, 441: 141754
- 102 Matsuo Y, Sekito K, Ashida Y, Inamoto J, Tamura N. *Chem-SusChem*, 2023, 16: e202201127
- 103 Wang YJ, Yu XW, Zhang P, Wang ZJ, Yan L, He L, Wang ZK, Shi ZQ. *Rare Met*, 2023, 42: 1545–1556
- 104 Wei Y, Tang B, Liang X, Zhang F, Tang Y. *Adv Mater*, 2023, 35: 2302086
- 105 Wan Y, Song K, Chen W, Qin C, Zhang X, Zhang J, Dai H, Hu Z, Yan P, Liu C, Sun S, Chou S-, Shen C. *Angew Chem Int Ed*, 2021, 60: 11481–11486
- 106 Asfaw HD, Kotronia A. *Cell Rep Phys Sci*, 2022, 3: 100693
- 107 Cheng Z, Guo L, Dong Q, Wang C, Yao Q, Gu X, Yang J, Qian Y. *Adv Energy Mater*, 2022, 12: 2202253
- 108 Kotronia A, van Ekeren WWA, Asfaw HD, Edström K. *Electrochim Commun*, 2023, 146: 107424
- 109 Li G, Wang H, Shi X, Yang C, Wang R, He B, Jin J, Gong Y, Tang A, Yang H. *Chem Commun*, 2022, 58: 11276–11279
- 110 Li WH, Li YM, Liu XF, Gu ZY, Liang HJ, Zhao XX, Guo JZ, Wu XL. *Adv Funct Mater*, 2022, 32: 2201038
- 111 Han F, Chen Y, Zhang J, Cai J, Xia X, Liu H. *ACS Appl Mater Interfaces*, 2021, 13: 10101–10109
- 112 Xiong L, Chen P, Chen Y, Han F, Zhang J, Liu H. *J Alloys Compd*, 2022, 911: 164871
- 113 Zhang K, Li D, Shao J, Jiang Y, Lv L, Shi Q, Qu Q, Zheng H. *ChemSusChem*, 2023, 16: e202300324
- 114 Shea JJ, Luo C. *ACS Appl Mater Interfaces*, 2020, 12: 5361–5380
- 115 Song Z, Zhou H. *Energy Environ Sci*, 2013, 6: 2280–2301
- 116 Hatakeyama-Sato K, Oyaizu K. *Chem Rev*, 2023, 123: 11336–11391
- 117 Suga T, Sugita S, Ohshiro H, Oyaizu K, Nishide H. *Adv Mater*, 2011,

- 23: 751–754
- 118 Wang Z, Zhu Q, Wang J, Jin F, Zhang P, Yan D, Cheng P, Chen Y, Zhang Z. *Sci China Chem*, 2022, 65: 2144–2162
- 119 Hudak NS. *J Phys Chem C*, 2014, 118: 5203–5215
- 120 Li Z, Tan J, Wang Y, Gao C, Wang Y, Ye M, Shen J. *Energy Environ Sci*, 2023, 16: 2398–2431
- 121 Kye H, Kang Y, Jang D, Kwon JE, Kim BG. *Adv Energy Sustain Res*, 2022, 3: 2200030
- 122 Wang F, Wang J, Li G, Guo Z, Chu J, Ai X, Song Z. *Energy Storage Mater*, 2022, 50: 658–667
- 123 Obrezkov FA, Fedina ES, Somova AI, Akkuratev AV, Stevenson KJ. *ACS Appl Energy Mater*, 2021, 4: 11827–11835
- 124 Raju V, Rani JV, Basak P. *Electrochim Acta*, 2020, 361: 137097
- 125 He F, Zhou Y, Chen X, Wang T, Zeng Y, Zhang J, Chen Z, Liu W, Gao P. *Chem Commun*, 2023, 59: 2787–2790
- 126 Tan Y, Chen Z, Tao Z, Wang A, Lai S, Yang Y. *Angew Chem Int Ed*, 2023, 62: e202217744
- 127 Wang HG, Wang H, Si Z, Li Q, Wu Q, Shao Q, Wu L, Liu Y, Wang Y, Song S, Zhang H. *Angew Chem Int Ed*, 2019, 58: 10204–10208
- 128 Kwon G, Ko Y, Kim Y, Kim K, Kang K. *Acc Chem Res*, 2021, 54: 4423–4433
- 129 Zhao Y, Ni M, Xu N, Li C, Ma Y, Zhang H, Chen Y. *Sci China Chem*, 2023, 66: 2683–2689
- 130 Zhang H, Xu D, Wang L, Ye Z, Chen B, Pei L, Wang Z, Cao Z, Shen J, Ye M. *Small*, 2021, 17: 2100902
- 131 Gu H, Zhong L, Shi G, Li J, Yu K, Li J, Zhang S, Zhu C, Chen S, Yang C, Kong Y, Chen C, Li S, Zhang J, Zhang L. *J Am Chem Soc*, 2021, 143: 8679–8688
- 132 Wang X, Li G, Han Y, Wang F, Chu J, Cai T, Wang B, Song Z. *ChemSusChem*, 2021, 14: 3174–3181
- 133 Wei B, Hong Y, Tang W, Guo M, He X, Tang C, Hu J, Fan C. *Chem Eng J*, 2023, 451: 138773
- 134 Zhang H, Zhong L, Xie J, Yang F, Liu X, Lu X. *Adv Mater*, 2021, 33: 2101857
- 135 Speer ME, Kolek M, Jassoy JJ, Heine J, Winter M, Bieker PM, Esser B. *Chem Commun*, 2015, 51: 15261–15264
- 136 Mishra SB, Abhijitha VG, Ramaprabhu S, Nanda BRK. *ACS Appl Energy Mater*, 2021, 4: 7786–7799
- 137 Zhang M, Zhong J, Zhu J, Kong W, Wang Y. *J Electroanal Chem*, 2022, 909: 116155
- 138 Gu J, Yuan Z, Wang H, Shen J, Ning J, Zhong Y, Hu Y. *Chem Eng J*, 2022, 448: 137711
- 139 Gao H, Xue L, Xin S, Goodenough JB. *Angew Chem Int Ed*, 2018, 57: 5449–5453
- 140 Chen Y, Manzhos S. *J Power Sources*, 2016, 336: 126–131
- 141 Bredas JL, Street GB. *Acc Chem Res*, 1985, 18: 309–315
- 142 Sun Z, Zhu K, Liu P, Li H, Jiao L. *Adv Funct Mater*, 2021, 31: 2107830
- 143 Sun Z, Zhu K, Liu P, Chen X, Li H, Jiao L. *Angew Chem Int Ed*, 2022, 61: e202211866
- 144 Zhu Y, Yin J, Emwas AH, Mohammed OF, Alshareef HN. *Adv Funct Mater*, 2021, 31: 2107523
- 145 Obrezkov FA, Shestakov AF, Vasil'ev SG, Stevenson KJ, Troshin PA. *J Mater Chem A*, 2021, 9: 2864–2871
- 146 Zhou R, Hou Z, Fan K, Wun CK, Liu Q, Lo TWB, Huang H, Zhang B. *J Power Sources*, 2023, 569: 232995
- 147 Xiu Y, Mauri A, Dinda S, Pramudya Y, Ding Z, Diemant T, Sarkar A, Wang L, Li Z, Wenzel W, Fichtner M, Zhao-Karger Z. *Angew Chem Int Ed*, 2023, 62: e202212339
- 148 Huang L, Yu Z, Wang L, Qin B, Cai F, Yuan Z, Luo Z. *J Energy Chem*, 2023, 83: 24–31
- 149 Hua F, Ruckenstein E. *Macromolecules*, 2005, 38: 888–898
- 150 Permpool T, Sirivat A, Aussawasathien D, Wannatong L. *Mat Res*, 2013, 16: 1020–1029
- 151 Lee M, Hong J, Lee B, Ku K, Lee S, Park CB, Kang K. *Green Chem*, 2017, 19: 2980–2985
- 152 Desmaizieres G, Perner V, Wassy D, Kolek M, Bieker P, Winter M, Esser B. *Batteries Supercaps*, 2023, 6: e202200464
- 153 Obrezkov FA, Somova AI, Fedina ES, Vasil'ev SG, Stevenson KJ, Troshin PA. *Energy Tech*, 2020, 9: 2000772
- 154 Yang Z, Huang X, Meng P, Jiang M, Wang Y, Yao Z, Zhang J, Sun B, Fu C. *Angew Chem Int Ed*, 2023, 62: e202216797
- 155 Zhang J, Liu H, Jia K, Li X, Liu X, Zhu L, He R, Wu F. *J Mater Chem A*, 2023, 11: 2711–2717
- 156 Ikhe AB, Seo JY, Park WB, Lee JW, Sohn KS, Pyo M. *J Power Sources*, 2021, 506: 230261
- 157 Suga T, Pu YJ, Kasatori S, Nishide H. *Macromolecules*, 2007, 40: 3167–3173
- 158 Kolek M, Otteny F, Schmidt P, Mück-Lichtenfeld C, Einholz C, Becking J, Schleicher E, Winter M, Bieker P, Esser B. *Energy Environ Sci*, 2017, 10: 2334–2341
- 159 Otteny F, Perner V, Wassy D, Kolek M, Bieker P, Winter M, Esser B. *ACS Sustain Chem Eng*, 2020, 8: 238–247
- 160 Dai G, Wang X, Qian Y, Niu Z, Zhu X, Ye J, Zhao Y, Zhang X. *Energy Storage Mater*, 2019, 16: 236–242
- 161 Obrezkov FA, Ramezankhani V, Zhidkov I, Traven VF, Kurmaev EZ, Stevenson KJ, Troshin PA. *J Phys Chem Lett*, 2019, 10: 5440–5445
- 162 Niu Z, Wu H, Liu L, Dai G, Xiong S, Zhao Y, Zhang X. *J Mater Chem A*, 2019, 7: 10581–10588
- 163 Škorjanc T, Shetty D, Olson MA, Trabolsi A. *ACS Appl Mater Interfaces*, 2019, 11: 6705–6716
- 164 Ikhe AB, Naveen N, Sohn KS, Pyo M. *Electrochim Acta*, 2018, 283: 393–400
- 165 Dai G, Liu Y, Niu Z, He P, Zhao Y, Zhang X, Zhou H. *Matter*, 2019, 1: 945–958
- 166 Hong H, Guo X, Zhu J, Wu Z, Li Q, Zhi C. *Sci China Chem*, 2024, 67: 247–259
- 167 Wang C, Xue S, Lei X, Wen J, Pan X, Zhang F, Zou C, Tang Y. *Chem Eng J*, 2023, 470: 144043
- 168 Gu S, Chen J, Hao R, Chen X, Wang Z, Hussain I, Liu G, Liu K, Gan Q, Li Z, Guo H, Li Y, Huang H, Liao K, Zhang K, Lu Z. *Chem Eng J*, 2023, 454: 139877
- 169 Liu Y, Lu Y, Khan AH, Wang G, Wang Y, Morag A, Wang Z, Chen G, Huang S, Chandrasekhar N, Sabagh I, Li D, Zhang P, Ma D, Brunner E, Yu M, Feng X. *Angew Chem Int Ed*, 2023, 62: e202306091
- 170 Sun W, Zhou C, Fan Y, He Y, Zhang H, Quan Z, Kong H, Fu F, Qin J, Shen Y, Chen H. *Angew Chem Int Ed*, 2023, 62: e202300158
- 171 Zeng Y, Zhou J, Zhang J, Liao Y, Sun C, Su Y, Gao P, Tan S. *Chem Commun*, 2023, 59: 4962–4965
- 172 Ye F, Liu Q, Dong H, Guan K, Chen Z, Ju N, Hu L. *Angew Chem Int Ed*, 2022, 61: e202214244
- 173 Wang H, Wu Q, Cheng L, Chen L, Li M, Zhu G. *Energy Storage Mater*, 2022, 52: 495–513
- 174 Walter M, Kravchyk KV, Böfer C, Widmer R, Kovalenko MV. *Adv Mater*, 2018, 30: 1705644
- 175 Reddy MA, Fichtner M. *J Mater Chem*, 2011, 21: 17059–17062
- 176 Zhang R, Ling C, Mizuno F. *Chem Commun*, 2015, 51: 1487–1490
- 177 Cao Z, Hu H, Ho D. *Adv Funct Mater*, 2022, 32: 2111805
- 178 Duay J, Lambert TN, Kelly M, Pineda-Dominguez I. *J Electrochem Soc*, 2019, 166: A687–A694
- 179 Li Q, Qiao Y, Guo S, Jiang K, Li Q, Wu J, Zhou H. *Joule*, 2018, 2: 1134–1145
- 180 Kwak KH, Suh HJ, Kim A, Park S, Song J, Li S, Kim Y, Jeong G, Kim H, Kim YJ. *Nano Energy*, 2019, 66: 104138
- 181 Chen Z, Cui H, Hou Y, Wang X, Jin X, Chen A, Yang Q, Wang D, Huang Z, Zhi C. *Chem*, 2022, 8: 2204–2216
- 182 Aubrey ML, Long JR. *J Am Chem Soc*, 2015, 137: 13594–13602
- 183 Wang G, Park JM, Kang T, Lee SJ, Park HS. *Small Methods*, 2023, 7: 2201440